FLYING ANIMAL INSPIRED BEHAVIOR-BASED GAP-AIMING AUTONOMOUS FLIGHT WITH A SMALL UNMANNED ROTORCRAFT IN A RESTRICTED MANEUVERABILITY ENVIRONMENT

A Dissertation

by

TRACI ANN SARMIENTO

Submitted to the Office of Graduate and Professional Studies of
Texas A&M University
in partial fulfillment of the requirements for the degree of

DOCTOR OF PHILOSOPHY

Chair of Committee,	Robin Murphy
Committee Members,	Yoonsuck Choe
	Dylan Shell
	Michael Smotherman
Head of Department,	Dilma Da Silva

August 2017

Major Subject: Computer Science

ABSTRACT

This dissertation research shows a small unmanned rotorcraft system with onboard processing and a vision sensor can produce autonomous, collision-free flight in a restricted maneuverability environment with no a priori knowledge by using a gap-aiming behavior inspired by flying animals. Current approaches to autonomous flight with small unmanned aerial systems (SUAS) concentrate on detecting and explicitly avoiding obstacles. In contrast, biology indicates that birds, bats, and insects do the opposite; they react to open spaces, or gaps in the environment, with a *gap_aiming* behavior. Using flying animals as inspiration a behavior-based robotics approach is taken to implement and test their observed gap-aiming behavior in three dimensions. Because biological studies were unclear whether the flying animals were reacting to the largest gap perceived, the closest gap perceived, or all of the gaps three approaches for the perceptual schema were explored in simulation: *detect_closest_gap*, *detect_largest_gap*, and *detect_all_gaps*. The result of these simulations was used in a proof-of-concept implementation on a 3DRobotics Solo quadrotor platform in an environment designed to represent the navigational difficulties found inside a restricted maneuverability environment. The motor schema is implemented with an artificial potential field to produce the action of aiming to the center of the gap. Through two sets of field trials totaling fifteen flights conducted with a small unmanned quadrotor, the gap-aiming behavior observed in flying animals is shown to produce repeatable autonomous, collision-free flight in a restricted maneuverability environment. Additionally, using the distance from the starting location to perceived gaps, the horizontal and vertical distance traveled, and the distance from the center of the gap

during traversal the implementation of the gap selection approach performs as intended, the three-dimensional movement produced by the motor schema and the accuracy of the motor schema are shown, respectively. This gap-aiming behavior provides the robotics community with the first known implementation of autonomous, collision-free flight on a small unmanned quadrotor without explicit obstacle detection and avoidance as seen with current implementations. Additionally, the testing environment described by quantitative metrics provides a benchmark for autonomous SUAS flight testing in confined environments. Finally, the success of the autonomous collision-free flight implementation on a small unmanned rotorcraft and field tested in a restricted maneuverability environment could have important societal impact in both the public and private sectors.

DEDICATION

To Andre, but for Michelle and her boys

ACKNOWLEDGMENTS

My time at Texas A&M University may have been short, but the list of mentors, colleagues, friends, and family I need to thank is long.

First, I would like to express my most sincere gratitude to my advisor, Dr. Robin Murphy. Your dedication, focus, and resiliency is to be admired. You pushed me to think bigger, work harder, dig deeper, and write better over these past three years. Thank you for taking on this "special case". To the rest of my committee members: thank you. Dr. Dylan Shell, you have a unique ability to provide feedback in a way that is both constructive and motivating. The time you took to dispense your point of view improved the outcome of this research. Dr. Michael Smotherman, I appreciate the insights you gave to refine my take on the ethological studies. Of course, touring your lab was one of the highlights of my time here. I can't decide whether working with bats, or robots is more amazing! Dr. Choe, thank you for taking the time to participate on my committee.

The number of people that fall into the colleagues and friends categories are too numerous to include here, but if you're reading this and consider yourself part of those groups please accept my heartfelt thank you.

And now, we come to family. Simply put, I am blessed. Even if I was given the opportunity to choose all those years ago, I could not have selected two better folks to be my parent. Lind-er and Dave, who are better known as Grandma and Grandpa these days, have been my biggest fans since day one. If I had to name the one thing that made all the difference, it was your expectations. Thank you for setting the bar high and providing me with the skills, opportunities, and love needed to vault over it.

Team Sarmiento: WE DID IT!!!! Eva, those exclamations are for you. ;) Lincoln, in our time here I've watched you turn from our toddler "Lincoln-big-boy-bigger" into

the amazing kindergarten graduate who wants to change his name to ”Abe”, so he can become President of the United States one day. I have no doubt you'll achieve that dream if you channel all that energy (especially your 0500 energy), and never lose the infectious giggle or the sparkle that lights up your eyes when you smile. Eva, my sweet baby Goo, you've turned into a young lady right before our eyes. You're quiet and introspective, but independent and fiercely loyal. With your heart and smarts, look out world! You told me last year you were going to visit Saturn to slide around its rings and I can't wait to wave to you as you launch into history. Finally, Andre. There's nothing to say except I could not have done this without you. Oh, but who are we kidding....I always have more to say. You have let me chase my dream over these last 10 years of marriage. We're looking at move number 5 through 3 states and 2 countries. We've added 2 kiddos, 2 dogs, and 3 cats to Team Sarmiento over the years, and said goodbye to irreplaceable members of our family. You've been my partner through it all and quietly taken care of our home, our kids, our pets, our parents, and me without complaint by reinventing yourself countless times. Here's to many more decades of adventures!

CONTRIBUTORS AND FUNDING SOURCES

Contributors

This work was supported by a dissertation committee consisting of Professor Robin Murphy [advisor], Professor Yoonsuck Choe, and Professor Dylan Shell of the Department of Computer Science and Engineering and Professor Michael Smotherman of the Department of Biology.

All work conducted for the dissertation was completed by the student independently.

Funding Sources

Graduate study was supported by the Department of Computer Science and Engineering at Texas A&M University.

NOMENCLATURE

SUAS	Small Unmanned Aerial System
MAV	Micro Aerial Vehicle
FOV	Field of View
APF	Artificial Potential Field
IBVS	Image-based Visual Servo Control
PBVS	Pose-based Visual Servo Control

TABLE OF CONTENTS

Page

LIST OF FIGURES

FIGURE Page

LIST OF TABLES

1. INTRODUCTION

This dissertation research implements a gap-aiming behavior for autonomous collision-free flight inspired by flying animals. In addition, it reports on field tests of the implementation in an environment simulating both the experimental environments seen in the ethological literature and the destruction of building interiors following a man-made, or natural disaster by employing quantitative metrics. The employment of small unmanned aerial systems (SUAS) to perform work in any of the three Ds [dirty, dangerous, or dull] [4] translates to reduced personal risk to humans from an unsafe environment, cost savings through reduced labor, and improvements in technologic support capabilities. The addition of autonomy to the system provides repeatable performance in the same scenario and removes the human factor that could lead to mishaps whether during training, or mission operation [5]. Specifically, a SUAS with the capability to operate autonomously and collision-free in an environment typical of the interior of an office building after a natural disaster has the potential to assist first responders and infrastructure engineers by providing imagery of the status of the interior, locating victims, or traversing areas too confined for a human.

These goals are met by answering the primary research question discussed in the following section. Section 1.2 provides insight into the need for small unmanned aerial systems to autonomously avoid collisions, why a review of the ethological literature on obstacle avoidance in flying animals was conducted, and the rationale behind the decision to conduct a study in simulation followed by field tests with the gap-aiming behavior implemented on a 3DRobotics Solo quadrotor platform. Section 1.3 defines the contributions the research provides and finally, Section 1.4 outlines the rest of the dissertation document.

1.1 Research Question

The primary research question to be addressed through the experimental study and proof-of-concept implementation conducted during the course of this dissertation research is:

Using flying-animal behavior as a guide, does a gap-aiming behavior implemented with an artificial potential field produce autonomous, collision-free flight on a small unmanned rotorcraft in a restricted maneuverability environment?

Autonomous control of SUAS is a developing area of research in the field of robotics with collision avoidance maintaining an important role in creating the autonomy. While systems have been developed and tested to autonomously fly indoors, none have been shown to match the performance, or emulate the gap-aiming behavior of flying animals in restricted maneuverability environments. This primary research question will attempt to determine if the gap-aiming behavior derived from a study of obstacle avoidance in flying animals can be transferred to provide autonomous collision-free flight of a small unmanned quadrotor in a restricted maneuverability environment. The gap-aiming behavior was implemented by taking a behavior-based robotics approach and tested through a study using simulation. The results of the simulation were implemented in a proof-of-concept on a 3DRobotics Solo quadrotor and tested in field experiments. The simulation and proof-of-concept hardware implementation are both described in detail in Chapter 6.

The primary research question was developed through observations made in the ethological literature about how flying animals avoid obstacles during flight. Two species of birds surveyed, the pigeon and starling, showed a preference for maneuvering through the largest visual gap in the environment when avoiding obstacles. The authors concluded this choice was made for safety reasons when traveling at higher flight speeds [6, 7]. Lin also noted that pigeons chose a centered flight path and would return to it after perform-

ing an avoidance maneuver [6]. In [8], blowflies also showed a preference for creating a nearly-centered flight path when avoiding obstacles. Because the literature was unclear whether flying animals were reacting to the closest, largest, or all of the gaps in their field of view (FOV) a simulation study was conducted and is described in Section 6.1. The simulation study provided insight into the best perceptual schema approach for a gap-aiming behavior on a small unmanned quadrotor, showing it is consistent with what was observed in the experiments performed with the flying animals and through field experiments it is sufficient to ensure collision-free flight in a restricted-maneuverability environment on a small unmanned quadrotor. Further details on the observations made from the review of literature are discussed in Section 4.1.

1.2 Flying Animal Behavior-based Autonomous SUAS

The ability of a SUAS to autonomously fly collision-free in a restricted maneuverability environment by implementing a gap-aiming behavior inspired by flying animals has not previously been investigated. Currently, obstacle avoidance for a teleoperated SUAS is hindered by the pilot's proficiency at flying the platform, the length of time before they become cognitively fatigued, and their capacity to gain and maintain awareness of the operational environment. While considerable research has been conducted on path planning to facilitate autonomous flight, this technique requires information about the environment a priori. Additionally, pre-defined paths created during traditional path planning do not take into account dynamic, or unseen obstacles making reactive control for autonomous collision-free flight desirable.

Animals conduct obstacle avoidance reactively, and therefore provide an existence proof for the belief that flight can be conducted collision-free at a high flight speed in an environment with closely spaced obstacles. Through designed experiments and observations in their natural habitat, researchers reported on the ability of birds, bats, and

insects to successfully navigate collision-free through restricted maneuverability environments. Reports on their capabilities show these flying animals do so with limited computational power and make decisions with incomplete and/or imperfect information about their environment. Three control rules were derived from the flying animal observations discussed in the literature review conducted in Chapter 3. These rules are described in detail in Chapter 4. The gap-aiming behavior designed from them was implemented using a behavior-based robotics approach to provide autonomous collision-free flight on a small unmanned quadrotor.

The gap-aiming behavior was implemented and tested in simulation through Study 1 to determine the best perceptual schema approach from three available options: *detect_closest_gap*, *detect_largest_gap*, and *detect_all_gaps*. The details of the simulation implementation are described in Chapter 5, Study 1 is outlined in Chapter 6, where the results are also presented. Because the platform may not act as expected, simulation removes the possibilities of damage to the environment, loss of the platform, or injury to the operator, therefore providing a safe environment for initial testing. Following the results of Study 1, a proof-of-concept was implemented on a 3DRobotics Solo quadrotor using the gap-aiming behavior to produce autonomous collision-free flight. Through field experiments, this proof-of-concept demonstrates the platform can achieve repeatable, autonomous, collision-free flight in an environment comparable to those observed in flying animal studies. The testing environment for the proof-of-concept was designed to simplify the perception problem, but still test the autonomous collision-free flight capabilities of the platform in three-dimensions in a restricted maneuverability environment.

1.3 Contributions of the Research

Answering the primary research question contributes to the fields of Artificial Intelligence, Robotics, and Ethology. Current research for autonomous collision-free flight on

SUASs is concentrated on the detection and avoidance of obstacles in the environment. Through a review of the ethological literature, observations were made about how birds, bats, and insects avoid obstacles in their environment. When compared to the current state of the art in obstacle avoidance for SUASs, the gap-aiming behavior used by the flying animals is dissimilar. Flying animals outperform the SUASs with faster flight speeds and smaller safety margins by using a single sense for perception with no need to maintain an internal representation of their environment. The research contributes to the field of artificial intelligence with the implementation of a novel artificial potential field (APF). This is the only known implementation of autonomous flight with an APF using no repulsive field. In this way, it extends AI's APF methodology to SUAS to produce autonomous flight. The research contributes to the robotics community by extending the corpus of behavior-based robotics applied to aerial vehicles for autonomous flight.

The experimental environments currently used to test the autonomous flight capabilities of SUASs are simplistic and described through language rather than metrics. This research tests the gap-aiming behavior implementation in an environment quantified by metrics from disaster robotics [9]. The field experiments are the first testing of an autonomous SUAS in an environment quantified with a comprehensive suite of metrics transferred fro disaster robotics. The implementation of this gap-aiming behavior on a small unmanned quadrotor may also be of interest to the ethological community. Results and observations of the completed experiments on this SUAS could lead to new theories of flying animal behaviors to investigate discussed in Section **??**. Additionally, because it was lacking the ethological literatures, the quantitative metrics used to define the flight environment could be useful when observing flying animal behavior.

The successful implementation of the gap-aiming behavior to provide autonomous collision-free flight in a restricted maneuverability environment could also have important societal impacts. In terms of public safety, autonomous collision-free flight beyond

line of sight has the potential to improve the reconnaissance capability for the military, intelligence community, and civilian agencies such as Homeland Security, law enforcement, and FEMA for disaster recovery. It could increase the speed and effectiveness of both the entry and clearing of buildings and structures, improve the assessment of a hostage situation, or provide hazardous materials identification without putting human, or animal lives at risk.

1.4 Organization of the Dissertation

The rest of this document is outlined in the following seven chapters. Chapter 2 discusses related work on SUASs. Chapter 3 provides a background on the ethological literature studied to determine how animals produce collision-free flight in their environment. Chapter 4 discusses the control rules derived from ethology and a behavior-based robotics approach taken to implement the gap-aiming behavior on a SUAS. The implementation details are provided in Chapter 5. Chapter 6 describes the simulation experiments, proof-of-concept implementation designed to answer the research primary question, and the results of them. Chapter 7 analyzes and discusses the findings of the research. Finally, Chapter 8 summarizes the dissertation research and provides avenues for future work.

2. RELATED WORK

Ensuring the safety of the platform, environment, and bystanders requires an SUAS operating in an indoor, highly confined space to autonomously fly collision-free. To put this work into context, it is important to understand the role reactive control for obstacle avoidance plays in the autonomous flight of SUASs, what the state of the art is in the field, what limitations exist in current implementations, and the experimental environment and metrics used for testing. Because this research took a behavior-based robotics approach for implementation, the discussion of the literature reviewed follows schema theory as described by Arkin [10], and Murphy [1]. Where possible, the primitive behaviors used for autonomous collision-free flight were identified and decomposed into the sensors, perceptual schemas, percepts, and motor schemas employed. These are the building blocks of primitive behaviors and their relationship to each other is illustrated in Figure 2.1. This figure shows how a *behavior* accepts inputs from one or more sensors, processes the sensing data via a *perceptual schema* to produce a percept, which produces a motor action via a *motor schema*.

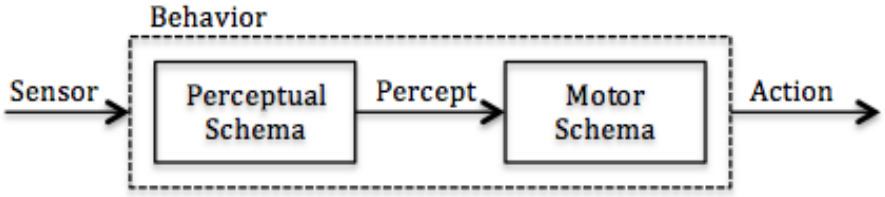

Figure 2.1: Depiction of behavior decomposition

The review covers eleven papers implementing an obstacle avoidance behavior. Obstacle avoidance implementations that follow the deliberative paradigm meaning, they exhibit

no reactive control and incorporate path planning and/or map creation to achieve obstacle avoidance were excluded. Additionally, work covering platforms that were not operated autonomously was also excluded.

The decomposition of the obstacle avoidance behavior resulted in isolation of two sensor categories utilized for perception, six perceptual schemas, twelve percepts, and eleven motor schemas. Following the schema theory discussion, the limitations of current implementations which explicitly detect and avoid obstacles are identified in Section 2.2. These limitation fall into two categories: operation in only two dimensions, and motor actions used to avoid obstacles not useful in restricted maneuverability environments. Finally, the experimental environments and metrics used for testing are discussed in Section 2.4. Conclusions about the current state of autonomous collision-free flight research for SUASs are drawn and areas of interest for this research are highlighted. The chapter concludes with a brief summary in Section 2.6.

2.1 Reactive Control of Obstacle Avoidance for SUAS

Reactive techniques for autonomous obstacle avoidance with SUASs make use of environmental percepts to act without requiring a formal representation of the world. The reactive paradigm has the ability to produce an action without a priori knowledge of the environment used in a planning step because a percept is immediately acted upon. Additionally, the existence of dynamic objects, or those initially not perceived, in an environment mean the world remains inconsistent through time. The need to continually update a world model, and reconstruct the plan is time-consuming and computationally expensive for deliberative methods. The remainder of this section is broken down into subsections corresponding to the building blocks of a primitive behavior used for reactive control and illustrated in Figure 2.1.

2.1.1 Sensors

Sensor use for implementing obstacle avoidance behavior in SUASs can be separated into two categories: passive and active. A sensor is considered passive when it collects data through energy received, like a camera. An active sensor emits energy and measures its interaction, like ultrasonic and laser implementations [11]. The categories each encompass multiple types of sensors chosen due to payload considerations, power availability, or percepts required for action. Eleven papers were surveyed, where seven employed passive sensors, and six active sensors. Two papers overlap categories because the authors used multiple sensors to collect data for obstacle avoidance purposes.

For obstacle avoidance, the most commonly used sensors are passive where 8 of the eleven papers surveyed used this type of sensor. Table 2.1 shows the papers surveyed where this category of sensor was employed and is further broken down into four specific types of sensors used by the authors surveyed. The choice of passive sensors may be due to their light weight when payload is a concern, low power consumption from their passive nature, or the specific percept required for the algorithm.

2.1.2 Perceptual Schemas and Percepts

Making use of the sensors described in the previous section, the collected data is forwarded to perceptual schemas to extract the percepts required by the specific obstacle avoidance implementation. The most common perceptual schema in ten of eleven papers surveyed, was detect_obstacle although the percept outputted to provide an appropriate motor action from the behavior was not always the same. The percepts extracted from the detect_obstacles perceptual schema were: distance_to_obstacle, obstacle_coordinates, distance_to_closest_obstacle, and obstacle_at_particular_depth. In [12] the perceptual schema takes input from eight ultrasonic sensors and a pair of wide-angle stereo cameras. The data from the cameras is used to determine obstacle coordinates while the perceptual

Table 2.1: Sensor use in SUASs for obstacle avoidance.

CATEGORY	TYPE	AUTHOR
Passive	Monocular Camera	Ross, et al., 2013
		Bills, Chen, & Saxena, 2011
	Stereo Camera	Nieuwenhuisen, Droeschel, Schneider, Holz, Labe, & Behnke, 2013
		Barry & Tedrake, 2015
		Hrabar, Sukhatme, Corke, Usher, & Roberts, 2005
	1D Camera	Zufferey & Floreano, 2006
	Directional Distance	Yuan, Recktenwald, & Mallot, 2009
Active	Ultrasonic	Gageik, Muller, & Montenegro, 2012
		Nieuwenhuisen, Droeschel, Schneider, Holz, Labe, & Behnke, 2013
		Bills, Chen, & Saxena, 2011
	Scanning Ladar	Scherer, Singh, Chamberlain, & Saripalli, 2007
	Laser Scanner	Grzonka, Grisetti, & Burgard, 2012
	2D Lidar	Merz & Kendoul, 2011

schema takes the ultrasonic data and provides the distance_to_the_obstacle. Similarly, [13] and [14] use directional distance and 2D lidar sensors, respectively, to provide data to the detect_obstacle perceptual schema. In turn, this perceptual schema calculates the distance_to_the_obstacle. Another perceptual schema utilized for obstacle avoidance is detect_altitude, where [15] and [13] are interested in perceiving the distance_to_the_ground, which could be stated as the platform height, in order to avoid collision with an obstacle below them, which could be the ground. The other perceptual schemas shown in Table 2.2, track_obstacle [12], classify_obstacle [16], classify_environment [17], and detect_wall [17], are one-off schemas used to identify percepts needed for specific obstacle avoidance implementations.

2.1.3 Motor Schemas

In the eleven papers surveyed, the description of the motor schemas identified to avoid obstacles are unique in in 7 of the eleven papers surveyed. There were two producing an

Table 2.2: Perceptual schemas used to extract percepts from sensor data.

PERCEPTUAL SCHEMA	PERCEPT	AUTHOR
detect_obstacle	distance_to_obstacle	Nieuwenhuisen, Droeschel, Schneider, Holz, Labe, & Behnke, 2013
		Grzonka, Grisetti, & Burgard, 2012
		Gageik,, Muller, & Montenegro, 2012
		Yuan, Recktenwald, & Mallot, 2009
		Scherer, Singh, Chamberlain, & Saripalli, 2007
		Bills, Chen, & Saxena, 2011
		Hrabar, Sukhatme, Corke, Usher, & Roberts, 2005
	obstacle_coordinates	Nieuwenhuisen, Droeschel, Schneider, Holz, Labe, & Behnke, 2013
	dist_closest_obstacle	Merz & Kendoul, 2011
	obstacle_at_set_depth	Barry & Tedrake, 2015
	optic_flow	Zufferey & Floreano, 2006
		Hrabar, Sukhatme, Corke, Usher, & Roberts, 2005
detect_altitude	distance_to_ground	Grzonka, Grisetti, & Burgard, 2012
	platform_height	Yuan, Recktenwald, & Mallot, 2009
track_obstacle	interest_points	Nieuwenhuisen, Droeschel, Schneider, Holz, Labe, & Behnke, 2013
classify_obstacle	image_features	Ross, et al., 2013
classify_environment	vanishing_cues	Bills, Chen, & Saxena, 2011
detect_wall	open_area distance_to_wall	Bills, Chen, & Saxena, 2011

optic flow percept for action [18, 19] and two whose action was to move_to_avoidance_waypoint [12, 14]. In the case of optic flow, the motor schema used was turn_away_from_higher_flow. For Zufferey [18], this allowed a fixed-wing platform to fly autonomously in circles in an open arena. The helicopter in [19] was able to remain centered while autonomously navigating an urban canyon. The AR Parrot in [17] navigated empty corridors and stairwells by using a move_opposite_obstacle motor schema. In [20] they did not explicitly discuss their motor actions, but viewing the video accompanying their research shows the same move_opposite_obstacle action used in [17]. Other authors chose to move_most_favorable_direction [13], adjust_to_learnt_heading [16], control_speed [21], or maintain_set_distance [15]. These motor schemas are all summarized in Table 2.3.

2.2 Limitations of Current Implementations

The limitations of the current reactive control implementations for obstacle avoidance can be split into two categories: operation in only two dimensions, and motor actions used to avoid obstacles not useful in restricted maneuverability environments. These two categories are discussed in the following subsections.

2.2.1 Operation in Two Dimensions

Of the ten current implementations of reactive control for collision-free flight surveyed, which detect obstacles for relative navigation purposes 6 operate in only two dimensions. Using LIDAR, Kukreti [22] detects obstacles in the environment computing a score for the path to each through the use of distance and angle measurements. The highest scoring movement is chosen and the SUAS is directed in two dimensions without altering the altitude. The gap-aiming behavior designed and implemented in this work operates in three dimensions because the ability to adjust altitude is a benefit of operating an aerial vehicle over a ground vehicle.

Table 2.3: Motor schemas used to avoid obstacles.

PERCEPTUAL SCHEMA	MOTOR SCHEMA	AUTHOR
detect_obstacle	move_to_avoidance_waypoint	Nieuwenhuisen, Droeschel, Schneider, Holz, Labe, & Behnke, 2013
		Merz & Kendoul, 2011
	turn_away_from_higher_flow	Hrabar, Sukhatme, Corke, Usher, & Roberts, 2005
		Zufferey & Floreano, 2006
	move_opposite_obstacle	Bills, Chen, & Saxena, 2011
		Barry & Tedrake, 2015
	move_most_favorable_direction	Yuan, Recktenwald, & Mallot, 2009
	speed_control	Scherer, Singh, Chamberlain, & Saripalli, 2007
	maintain_safe_distance	Gageik,, Muller, & Montenegro, 2012
classify_obstacle	adjust_to_learnt_heading	Ross, et al., 2013
detect_altitude	Not defined	Grzonka, Grisetti, & Burgard, 2012
	adjust_altitude	Yuan, Recktenwald, & Mallot, 2009
track_obstacle	Not defined	Nieuwenhuisen, Droeschel, Schneider, Holz, Labe, & Behnke, 2013
classify_environment	move_to_vanishing_point move_up_staircase	Bills, Chen, & Saxena, 2011
detect_wall	turn_to_most_open	Bills, Chen, & Saxena, 2011

2.2.2 Motor Actions Useless in Restricted Maneuverability Environments

In an indoor disaster environment the open area required for maneuvering, or the threshold distance from the obstacle required in the following two implementations likely does not exist. To autonomously navigate indoors, Winkvist used LIDAR to detect obstacles, then performed a banking maneuver to the most open area until the object was no longer considered a threat [23]. Using sonar, Bills detected an obstacle and moved the SUAS in the opposite direction until the obstacle is further than a preset threshold. Neither of these implementations was tested with an environment with closely spaced obstacles representative of the restricted maneuverability they might encounter indoors after a disaster.

2.3 Reaction: Obstacles versus Gaps

Current approaches to autonomous flight with SUAS concentrate on detecting and explicitly avoiding obstacles. In contrast, biology indicates that birds, bats, and insects do the opposite; they react to open spaces, or gaps in the environment. While SUASs have been developed and tested to autonomously fly indoors [15, 23, 22, 17, 24, 25, 26], none of these emulate the gap-aiming behavior of flying animals. To produce collision-free autonomous flight, this work implements a *gap_aiming* behavior inspired by flying animals to perceive gaps in the environment and react to them through the use of an artificial potential field, which produces action in three-dimensions.

2.4 Experimental Environments and Metrics

None of the autonomous obstacle avoidance capabilities were tested in highly confined experimental environments representative of what might be encountered in the interior of a building following a natural disaster. Of the eleven papers surveyed, six platforms were tested outdoors and seven were tested indoors, where two of the platforms overlapped

Table 2.4: Summary of environments used for testing.

ENVIRO TYPE	OBSTACLES	AUTHORS
Indoor	Lab with 1 fixed and 1 movable wall	Gageik,, Muller, & Montenegro, 2012
	Corridor with 1 dynamic obstacle	Grzonka, Grisetti, & Burgard, 2012
	Corridor with a barrel	Lee, Di Cicco, Grisetti, & Lee, 2016
	Simulation of corridor and maze Hallway with table	Yuan, Recktenwald, & Mallot, 2009
	Corridor with people, or boxes	Alvarez, Paz, Sterm, & Cremers, 2016
	Corridor and staircase	Bills, Chen, & Saxena, 2011
	Open arena	Zufferey & Floreano, 2006
Outdoor	Parking lot with building and slow moving sheet	Nieuwenhuisen, Droeschel, Schneider, Holz, Labe, & Behnke, 2013
	Field with tree, or goal post	Barry & Tedrake, 2015
	Field with trees, bushes, tower, fences, building, and vehicles	Merz & Kendoul, 2011
	Forest with 1 tree every 3x3 meters	Ross, et al., 2013
	Poles, wires, trees, and buildings	Scherer, Singh, Chamberlain, & Saripalli, 2007
	Open field with trees on one side Tower and carriage form urban canyon	Hrabar, Sukhatme, Corke, Usher, & Roberts, 2005

categories. Table 2.4 summarizes the testing environment for each implementation. In six of the seven indoor testing environments beyond the structure of the building there was either one obstacle [27, 15, 13, 25], or none [17, 18]. The other indoor environment used two obstacles that were either people, or boxes in a corridor placed side-by-side [26]. For the outdoor environments, three of the six had one obstacle [12, 20], or two [19]. The other three contained only trees [16], or a combination of trees, buildings, fences, and wires [14, 21].

Additionally, there were no consistent metrics used to define the experimental envi-

ronment, or to assess the success of an obstacle avoidance implementation. For all of the papers surveyed the environments were described as indoor, or outdoor and, if obstacles were present they were named. In the case of Yuan [13], the environment was described in the text as 'maze-like' and a picture was provided. The outdoor environments in [21], [12], and [14] identified the obstacles, but did not provide numbers, or spacing. The lack of description and quantitative metrics to define the environment makes the recreation of the testing environment impossible and raises questions about how the obstacle avoidance algorithms would perform in highly confined environments.

2.5 Conclusions

Implementations of autonomous collision-free flight for SUASs make use of a variety of sensors, which overwhelmingly employ detect_obstacle as the perceptual schema in ten of eleven cases, and extract the distance_to_obstacle in seven of those ten cases. This data is summarized in Table 2.2. The implementations diverge in their use of motor schemas to avoid the detected obstacles. While the two using optic flow as a percept to employ a turn_away_from_higher_flow motor schema reflect the centering response in honeybees and blowflies [28, 8] none of the other motor schemas were observed in the ethological literature.

Current implementations which only operate in two dimensions do not take advantage of the benefit aerial vehicles have over ground vehicles of adjusting their altitude for collision-free flight. Additionally, implementations which require an open area for avoidance, or a distance threshold to any obstacle are not suitable for restricted maneuverability environments. Finally, the experimental environments were too simplistic. Besides the lack of obstacles in the experimental environments, there was no recognized definition of clutter, or metrics used to quantify it.

2.6 Summary

In summary, this chapter discussed the importance of the role reactive obstacle avoidance plays in the autonomous collision-free flight of SUASs, described the perceptual schemas, percepts, and motor schemas used to implement obstacle avoidance on SUAS, the limitations of the current implementations, and the unquantified environments used for testing. Overall, the behaviors employed to explicitly detect and avoid obstacles in the environment do not match what was observed in a review of the ethological literature discussed in the following chapter. Additionally, the testing environments described are simplistic, have no consensus on the definition of clutter, do not adequately model the deconstruction found in an indoor environment following a natural disaster, and lack quantitative metrics necessary for evaluation and recreation.

3. BACKGROUND: FLYING ANIMALS

With the knowledge that flying animals outperform existing obstacle avoidance implementations on SUAS discussed in the previous chapter, flying animals were turned to for inspiration to answer the question: what are they doing differently? A review of twenty-three papers in the ethological literature was conducted and framed by schema theory. The perceptual schema portion of the primitive behaviors identified during the review are beyond the scope of this research, but are included in Section 3.3 because they may be of interest to the reader, or for future work. The fourteen motor schemas identified as part of the five primitive behaviors are discussed in Section 3.5. Four observations from the review of literature are introduced in Section 3.6 and the two observations specifically incorporated in the design of the gap-aiming behavior used in this research are discussed in Section 3.7.

3.1 Introduction to Ethological Literature Review

Animals have been used to inspire robotic control, design, and communication. In [29], the successful control of their legged robot's locomotion was derived from walking animals. The design of the robotic fish described in [30] was based on the "swimming skills and anatomic structure of a fish". To perform intrusion detection in [31], the social and communication systems of primates were applied to mobile robotic sensors patrolling large areas.

Because flying animals outperform existing SUAS, using a single sense to fly faster through clutter, a review of the ethological literature on obstacle avoidance in birds, bats, and insects was conducted. The intention was to gain an understanding of how flying animals physically respond to an obstacle to avoid collisions. The fact that flying animals serve as an existence proof means this knowledge could lead to the creation of biologically-

inspired behaviors to control a SUAS to improve the speed and accuracy when navigating in cluttered environments.

During controlled flights, the big brown bat successfully sensed and avoided vertical wires at speeds averaging up to 5.0 m/s [32]. Pigeons can reach cruising speeds greater than 10.0 m/s in open spaces and were shown to maintain an average flight speed of 4.38 m/s in a cluttered, indoor corridor used for experimentation [6]. Currently, successful implementations of collision avoidance on autonomous SUAS do not reach the flight speeds seen in animals, may require multiple modes of sensing to handle changing environments, or must collect and keep information about the environment to attain collision-free navigation. In Shen [33], a micro aerial vehicle (MAV) achieved autonomous navigation at an average speed of 1.5 m/s while traversing through building openings to fly both in and outdoors. This MAV required fusion of an IMU, laser scanner, stereo cameras, pressure altimeter, magnetometer, and a GPS receiver to ensure an accurate position estimation for autonomous flight due to the failure of certain sensors in changing lighting conditions. Additionally, a local map was maintained to ensure the platform did not drift while hovering. Ross, et al. also implemented an autonomous MAV, which successfully navigated with a single camera, at an average speed of 1.5 m/s, through a forest after conducting three rounds of imitation learning from an expert pilot [16].

Twenty-three papers from the ethological literature were surveyed in order to gain an understanding of the behaviors used by bats, birds, and insects. Papers were excluded if they were outside the ethological literature, the animal did not fly, or if neither a perception for obstacle detection nor motor action for obstacle avoidance was discussed. This review will frame the discussion of the literature using behavioral control terminology which reuses ethological terms [10], [1]. A *behavior* accepts inputs from one or more sensors, processes the sensing data via a *perceptual schema* to produce a *percept* which produces a motor action via a *motor schema* as illustrated in Figure 3.1.

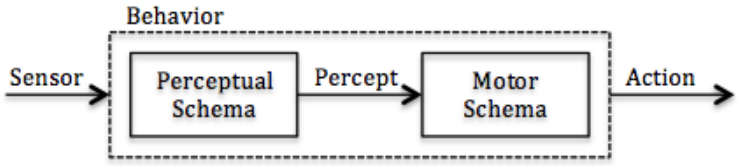

Figure 3.1: Behavior depicting primitive building blocks

The twenty-three papers were reviewed to extract the primitive behaviors used by flying animals to accomplish high-level tasks. Where able, these behaviors were decomposed into the building blocks depicted in Figure 3.1 and described above. Overall, five primitive behaviors were identified: avoid_object, obtain_food, evade_predator, track_mate, and center_flight. The perceptual schemas defined are divided into two categories: those to derive information from the environment and the adaptations used to improve the environmental information retrieved. Environmental sensing through passive means in birds and insects was discussed in ten of the twenty-three papers, while four papers discussed its use in bats. Twelve papers explored use of active sensing in birds and bats. Animals perceive through the use of different perceptual schemas, in this review eight different perceptual schemas were identified and are listed in Table 3.2 with descriptions to follow. In eight of the papers surveyed, when an object was initially detected, the animal adapted its normal use of vision, or sonar, to increase or improve its information about the object. Finally, eighteen papers provided insight into motor schemas used by birds, bats, and insects to avoid an object, obtain food, evade a predator, track a mate, or center their flight.

The rest of the discussion is organized as follows: Section 3.2 describes the sensors employed by the flying animals, Section 3.3 describes the perceptual schemas used for environmental sensing, Section 3.4 describes the ways flying animals adapt their sensing, Section 3.5 describes the motor schemas used in the five behaviors when they were described in the literature, and Section 3.6 defines the observations made about the flying

animals surveyed and concludes the background discussion.

3.2 Sensors Used for Detection

Due to the dynamic nature of their environment, flying animals need to continually monitor their surroundings to ensure collision-free navigation and survival, while gathering information to self-orient. This monitoring can be done through the use of one, or multiple sensors. Birds use vision to passively monitor; however, certain species were shown to use vocalizations. These vocalizations are a more crude form of the biological sonar found in bats. This sonar-like active sensing in birds is used when flying in the darkness encountered in caves where they roost. The species of bats surveyed use sonar to actively monitor their environment, but two species surveyed make use of vision in lighted scenarios. Eklof concludes bats sense through vision for three main reasons: to navigate over long distances because the range of echolocation is short, to distinguish color and brightness for foraging purposes, and to detect the amount of ambient light in the environment to either determine the time of day, or the increased danger of predation on moonlit nights [34]. The four insects surveyed and identified in Table 3.1 rely solely on vision for sensing [35, 8, 28, 36].

During the review, two types of sensors and three tasks required of the flying animals were identified. Table 3.1 depicts the two types of sensors surveyed and the flying animals using them to succeed at one of three tasks. Of the twenty-three papers surveyed, fourteen papers discussed passive sensing through vision where collision-free navigation was mentioned in thirteen, self-orientation in four, and survival in three. Use of sonar for active sensing was discussed in twelve papers where eleven covered collision-free navigation, three mentioned survival, and none mentioned self-orientation. The following subsections will discuss the sensing used for these tasks in more detail.

Sensor	Task	Animal
Passive	Collision-free Navigation	Pigeon [6]
		Zebra Finch [37]
		Starling [7]
		Budgerigar [38]
		Honeybee [35, 28]
		Blowfly [8]
		Hoverfly [28]
		Locust [36]
		Little Brown Bat [39, 40, 41]
		Greater Spear-nosed Bat and Short-tailed Fruit Bat [42]
	Self-orientation	Honeybee [35, 43]
		Blowfly [8]
		Hoverfly [28]
	Survival	Pigeon [6]
		Honeybee [35]
		Greater Spear-nosed Bat and Short-tailed Fruit Bat [42]
Active	Collision-free Navigation	Big Brown Bat [32, 44, 45]
		Little Brown Bat [41]
		Greater Spear-nosed Bat and Short-tailed Fruit Bat [42]
		Hipposiderid Bat [46]
		Mexican Leaf-nosed Bat [47]
		Unnamed Bats [48, 49]
		Cave Swiftlet [50]
		Oil Bird [51]
	Survival	Big Brown Bat [44, 45, 52]

Table 3.1: Sensors used to complete different tasks corresponding to a specific flying animal.

3.2.1 Passive Sensing Through Vision

Although they may need to perceive different things in their environment, four species of birds, four species of insects, and three species of bats surveyed all passively sense through vision. Of the twenty-three papers surveyed the use of vision was discussed in fourteen. In thirteen of the fourteen papers vision contributed to collision-free navigation, four papers dealt with self-orientation, and three discussed perception for survival.

Guided by vision, collision-free navigation is extremely important to flying animals because they have the opportunity to come into contact with man-made structures, other flying animals, vegetation, or other naturally occurring objects in their environment on a daily basis. The speed of flight adds to the challenge for birds, insects, and bats to navigate collision-free. In [53] the authors surveyed articles discussing collisions between birds and bats, and man-made structures where the outcome was death of the animal either through the collision itself, or via electrocution when the object was electrified. The penalty for collision is not always as severe as death; however, when injuries like bone fractures and internal bleeding are sustained in birds the probability of being captured by a predator increases [54]. The pigeon [6], zebra finch [37], starling [7], budgerigar [38], honeybee [35, 28], blowfly [8], hoverfly [28], locust [36], little brown bat [39], [40], [41], and the greater spear-nosed and short-tailed fruit bats [42] all use vision to complete the task of collision-free navigation.

Self-orientation, or knowing your own position in the world, is accomplished through vision in the honeybee [35, 43], blowfly [8], and hoverfly [28]. This capability is important to blowflies for determining their flight velocity [8], honeybees to center their flight path [35, 43], and hoverflies for mating purposes [28].

To survive, a flying animal must both feed and avoid becoming food for a predator. The pigeon [6], honeybee [35], and the greater spear-nosed and short-tailed fruit bats [42] all

use vision for the task of survival. Being at risk from other aerial predators means pigeons vision must detect these predators in the environment [6]. To ensure survival of themselves and their hive-mates, the honeybee must know and be able to return to the location of a food source [35]. Much like pigeons, the greater spear-nosed and short-tailed fruit bats must be able to detect predators when resting during the daylight hours for survival [42].

3.2.2 Active Sensing Through Sonar

The use of sonar for perception is typically attributed to bats; however, two species of birds surveyed also use a more crude version of sonar calls for echolocation [51], [50]. Of the twenty-three papers surveyed, twelve papers discussed sonar use with ten concentrating on different species of bats and two on birds. The use of sonar for collision-free navigation was discussed in eleven and survival in three, with no paper describing the use of sonar for self-orientation.

Bats, and species of birds which actively sense through sonar must navigate collision-free. As discussed in Subsection 3.2.1, collisions between bats and man-made structures like wind turbines, communication towers, windows, and power lines resulting in the death of the animal [53], [55]. The big brown bat, little brown bat, greater spear-nosed and short-tailed fruit bats, hipposiderid bat, Mexican leaf-nosed bat, other unnamed bats, cave swiftlet, and oil bird all use sonar to produce collision-free navigation.

Bats must ingest around 110 percent of their body weight in food each day and, due to the energy consumption of flight, likely would not survive more than twenty-four hours without any food. To ensure its survival, the big brown bat uses sonar to detect prey while foraging [44, 45].

3.3 Perceptual Schemas: Environment

Table 3.2 summarizes the perceptual schemas observed and discussed in the ethological literature. The specific percepts produced by the perceptual schemas and used by

the flying animals are shown in the table. These perceptual schemas would be implemented as the computational processes operating on the sensor output for a SUAS. In turn, they would produce a percept for action. The papers suggest eight perceptual schemas: detect_object, detect_altitude, distance_flown, detect_predator, detect_prey, detect_mate, detect_walls, and adapt_sensing. All of these perceptual schemas will be discussed in the subsections below.

3.3.1 Perceptual Schema: detect_object

Detecting objects was described in nineteen of the twenty-three papers covering five birds, four insects, six named bats, and seventeen unnamed bats. A perceptual schema produces percepts, which are not the same for every animal. These percepts are fed into a motor schema, sometimes from multiple perceptual schemas, to create a behavior. For the detect_object perceptual schema there were five percepts identified as information required by these animals to produce the desired motor action to avoid an obstacle.

3.3.1.1 Detecting Moving and Stationary Objects

Through flicker-fusion, at frequencies from 116 to 146 Hz, pigeons are able to perceive rapid motion in flight and therefore distinguish an object in motion from stationary ones. This rate of flicker-fusion, higher than the human average of 60Hz, allows pigeons to view smooth movement of objects instead of these objects appearing to move in a jerking manner [6]. Like pigeons, hoverflies also use optic flow to detect moving obstacles while they are in motion by recognizing the inconsistent flow produced by a moving object compared to a stationary one in the scene [28]. Optic flow is described as the change of structured light in the image on the retina due to a relative motion between the eyeball and the scene [56]. In [42], Chase suggests certain species of bat may first use vision as a passive sensor to detect silent, but moving obstacles before utilizing echolocation to derive the information they need to respond appropriately. Nocturnal birds, like the oil bird, make

Perceptual Schema	Percept	Animal
detect_object	moving_object	Pigeon [6]
		Hoverfly [28]
		Greater Spear-nosed Bat and Short-tailed Fruit Bat [42]
		Oil Bird [51]
	stationary_object	Cave Swiftlet [50]
		Blowfly [8]
		Little Brown Bat [39, 41]
		Greater Spear-nosed Bat and Short-tailed Fruit Bat [42]
		Mexican Leaf-nosed Bat [47]
		Unnamed Bat(s) [49]
	distance_to_object	Pigeon [6]
		Zebra Finch [37]
		Honeybee [35, 28]
		Blowfly [8]
	gap_size	Pigeon [6]
		Zebra Finch [37]
		Starling [7]
		Big Brown Bat [32, 45]
	object_size	Unnamed Bat(s) [48, 49]
	view_subtended	Locust [36]
detect_altitude	angular_velocity	Honeybee [28]
		Blowfly [8]
distance_flown	image_motion	Honeybee [35]
detect_predator	predator_present	Pigeon [6]
		Greater Spear-nosed Bat and Short-tailed Fruit Bat [42]
detect_prey	prey_present	Big Brown Bat [44, 45, 52]
detect_mate	mate_present	Hoverfly [28]
detect_walls	lateral_image_motion	Budgerigar [38]
		Honeybee [43]
		Blowfly [8]
adapt_sensing	distance_to_object	Zebra Finch [37]
		Hipposiderid Bat [46]
		Big Brown Bat [44, 32]
	stationary_object distance_to_object	Blowfly [8]
	moving_object	Greater Spear-nosed Bat and Short-tailed Fruit Bat [42]
	gap_size	Big Brown Bat [45]
	altitude	Little Brown Bat [41]

Table 3.2: Perceptual schemas used by specific flying animals to perceive information about the environment.

use of verbalizations to fly in near-darkness. They emit sharp clicks in short bursts while flying in a dark cave allowing them to avoid both the walls and other animals in moving flight [51].

The cave swiftlet uses brief clicks, audible to humans, to echolocate in darkness allowing them to avoid stationary objects in the caves where they roost [50]. Blowflies tend to prefer flight in the center of a tunnel, but initiate turns in a narrow s-shaped pattern to avoid stationary obstacles in their flight path. They detect these stationary objects through saccadic turns to intentionally produce changes in the optic flow [8]. When visual cues are available, the little brown bat uses vision to navigate and avoid obstacles; however, the visibility of the obstacles and the light intensity greatly affect the bats' ability to avoid collisions [39]. Additionally, the little brown bat uses sonar on the approach and navigation through a man-made barrier during experimentation in [41] showcasing their ability to detect and avoid stationary objects through echolocation. During high-illumination levels, the number of collisions with stationary obstacles increases, but at low-illumination when the scene is highly contrasted the little brown bat is able to use patterned visual cues to detect these stationary objects and avoid collisions [41]. Much like the little brown bat's use of vision, this same phenomenon was shown in [42] where the greater spear-nosed and the short-tailed fruit bats used vision to detect and avoid non-luminous objects in their environment. Experimental trials of the Mexican leaf-nosed bat with and without the use of vision showed no significant difference in their ability to detect stationary objects [47]. The thirteen unnamed species of bats in [49] detected and avoided a small stationary object when exiting their caves. The authors were using this experimental setup to show the bats still relied on echolocation in familiar situations rather than spatial memory as researchers previously thought.

3.3.1.2 Distance to an Object

During experimentation, the zebra finch flew at speeds up to 3.5 m/s requiring a fast method of perceiving information from the environment. Zebra finches use optic flow to detect the distance from themselves to an object, then use this information to execute collision avoidance turns [37]. Bees also measure the distance from themselves to the object by using optic flow, which provides them information about the speed of the image with respect to their position and movement in the environment [43], [28]. [36] describes how locusts measure both the speed of an object and the time to collision to judge the distance between themselves and an object. This helps them decide whether they will perform a turn, land, or simply glide.

3.3.1.3 Determining Gap Size

Pigeons, zebra finches, and starlings use optic flow to determine the size of the gap between objects [6], [37], [7]. Because pigeons cruise at speeds greater than 10 m/s, lack depth perception due to a narrow binocular field of view (FOV), and their visual acuity is poor they aim for the largest gap between objects by using optic flow to determine the gap size [6]. In [7] starlings were shown to prefer the larger visual gaps when their hunger was at a lower level, but would traverse a narrow gap when obtaining food became more important. Zebra finches make decisions about deviating from their planned path when presented with the possibility of collision from information they perceive through optic flow [37]. In [45], the big brown bat shifts the aim of its sonar from one side of a net opening to the other, collecting echoes, to determine the size of the gap and its traversability. [32] also discussed gap size determination through echolocation in big brown bats noting the smaller gap sizes required more accurate knowledge of the object positions to successfully avoid collisions.

3.3.1.4 Determining Object Size

[49] observed a mix of thirteen species of bats using the echo-amplitude and sonar aperture of their acoustic echoes to perceive the size of an object.

3.3.1.5 Determining Percent of View Subtended

Through experiments intended to determine the timing of obstacle avoidance in locusts, the authors of [36] concluded that maneuvers were initiated when at least 10 degrees of the locusts field of view was subtended by an obstacle. The size of the obstacle had no effect on the response; however, the speed of the obstacle did correlate to the magnitude of the response.

3.3.2 Perceptual Schema: Others

Besides the detect_object perceptual schema previously discussed there are six others described in the following subsections.

3.3.2.1 Detecting Altitude

Using the angular velocity measurement from optic flow both honeybees and blowflies are aware of their altitude. Honeybees use this information to hold the value constant as they decrease altitude for landing [28]. Blowflies use the information to maintain a constant altitude when flying in both open and cluttered spaces [8]

3.3.2.2 Determining Distance Flown

Through the use of optic flow, honeybees determine the distance flown to arrive at a food source once it has returned to the hive. The bee then relays this distance to its hivemates through dance, so they may also locate the food source [35].

3.3.2.3 Detecting Predators

Using information perceived through vision, pigeons, greater spear-nosed bats, and short-tailed fruit bats are able to detect predators in their environment [6], [42]. Pigeons have a 300 degree panoramic field of view (FOV) adapted for predator detection [6]. [42] suggested the greater spear-nosed and short-tailed fruit bat both use vision as a passive-surveillance system for detecting predators while at rest. This use of a passive surveillance system allows themt o conserve energy, therefore reducing their foraging requirement.

3.3.2.4 Detecting Prey

To ensure its survival, the big brown bat uses sonar to detect prey while foraging. This active sensing allows the bats to pursue and eventually intercept the prey [44]. The broad beam of their sonar would allow the big brown bat to gather information about all of the objects in the scene simultaneously, but instead they separate the tasks of obstacle avoidance from prey detection by directional aiming to sequentially scan the environment [45]. The specimens tested in [52] were recorded capturing free-flying insects in an attempt to determine the pursuit strategies employed by the big brown bat.

3.3.2.5 Detecting a Mate

In hoverflies, optical flow is used to provide them the ability to track an object in their surroundings. By tracking their mate the male hoverfly is able to produce a flight path which makes it appear he is not moving. This allows him the element of surprise during mating [28].

3.3.2.6 Detecting Walls

When flying through narrow passages the budgerigar uses optic flow information to detect the edges of its flight environment. Additionally, it is suspected the birds may also use geometric cues from the shape of the environment to navigate when optic flow

information is unavailable [38]. Both honeybees and blowflies attempt to maintain a flight path centered in a tunnel by ensuring the walls of the tunnel remain equidistant from them [28, 8].

3.4 Perceptual Schemas: Adaptive Sensing

The previous section described perceptual schemas for environmental sensing. The following subsections will cover adaptations birds, bats, and insects make to their sensing frequency and coverage in order to increase and/or improve their knowledge of the environment.

3.4.1 Distance to an Object

The zebra finch uses optic flow information to perceive information about its environment; however, in order for the information to be useful the optic flow perceived during rotational flight must be separated from the optic flow obtained during translational flight. To separate the two types of optic flow, the zebra finch uses a strategy to stabilize its gaze during flight. This stabilization allows it to extract the rotational optic flow using only the translational information to estimate distance [37].

The hipposiderid bat increases the number of calls and decreases the duration of each call emitted when flying in a cluttered environment to reduce the overlap of echoes. Additionally, Gustafson [46] showed these bats compensate for the Doppler shifts caused due to their flight by lowering the emission frequency of their calls. Sandig [32] found when the big brown bat was flying through a more cluttered environment, specifically where the obstacles were close together, their echolocation behavior changed. As the difficulty of navigation increased, so did the number of groups of calls and the number of calls within each group. In addition, as the distance between a bat and an object decreased the number of calls per group increased. The increase in pulses emitted improved the target localization accuracy. While observed flying in the forest in [44], the big brown bat emitted more

calls that were more closely space in time. This call pattern provides more echoes, which helps the bat perceive further information from the environment.

3.4.2 Detecting Moving and Stationary Objects

In the case of blowflies, they adapt their visual sensing during flight by incorporating saccadic head and body turns to derive more information about the environment. This is especially noticeable due to the increased frequency and amplitude of the saccades when the insect is close to an object. The sideways motion experienced after a saccade leads to extraction of depth information. Additionally, these movements are of the greatest need when the insect encounters a static object and needs to artificially create flow to drive the necessary percepts [8]. The greater spear-nosed bat and short-tailed fruit bat use vision for detecting predators while at rest. If a predator is detected moving in the environment through vision, then the bat will begin actively monitoring through the use sonar to accurately locate the intruder [42].

3.4.3 Determining Gap Size and Altitude

When confronted with a cluttered environment in [45], the big brown bat shifted its gaze to sequentially inspect objects that were within close proximity of each other. This technique is similar to the saccades described in insects and birds above. When attempting to land, the little brown bat will increase its pulse emission rate at a consistent distance from the surface which it determines through the received echoes. This increase in emission helps the bat more accurately target the landing zone [41].

3.5 Motor Schemas

Section 3.3 and Section 3.4 discussed the perceptual schemas flying animals use and the percepts produced. These percepts are then fed into motor schemas to create the desired action of the behavior. In the twenty-three papers reviewed five behaviors emerged with

fourteen motor schemas. The details of these behaviors and motor schemas are described in the following subsections and illustrated in Table 3.3.

3.5.1 Avoid Objects

Avoiding objects perceived in the environment requires a change to an animals' current flight trajectory with an adjustment in their direction, speed, or altitude. Understanding when and how these adjustments are made is required to effectively transfer the strategies flying animals use to accomplish high-level tasks to a SUAS for the same purpose.

3.5.1.1 Motor Schema: aim_gap_center

When pigeons detect an object, or multiple objects in their path they begin to adjust their flight path approximately 1.5 meters before they reach the object. They reduce their average flight speed to perform avoidance maneuvers when they are flying in a cluttered environment. The slower speed of their flight forces them to increase the frequency of their wing beats as compensation to stay airborne. While they choose the largest visual gap when in fast flight, instead of the closest, they also show preference for reducing the steering required to keep their path close to a straight-line [6]. Starlings also tended to choose flight through the largest visual gap when adjustments are required in their flight path due to objects; however, when they are hungrier they choose to accept the risk of flying through a smaller gap to obtain food [7]. When confronted with a cluttered environment, like a forest, the big brown bat reduces its speed to provide more time to collect additional information and adjust its flight path to avoid an object [44]. The need to more accurately sense the environment arises because the clutter causes a reduction in gap size. Regardless of the gap size or the speed they are traveling, the big brown bat begins avoidance maneuvers 1.5 to 1.0 meters from a detected object. As the gap sizes between stretched wires decreased during experimentation in [32], the big brown bat adjusted its flight path by increasing altitude, which also reduced speed. The smaller gaps require bet-

Behavior	Perceptual Schema	Percept	Motor Schema	Animal
avoid_ object	detect_object	object_size	Not Defined	Unnamed Bats [49]
		gap_size	aim_gap_center	Pigeon [6] Starling [7] Big Brown Bat[44, 32]
		distance_to_object		Pigeon[6] Honeybee[43]
		view_subtended	turn_brake or turn_speed	Locust [36]
	detect_altitude	angular_velocity	maintain_angular _velocity	Honeybee [28]
	adapt_sensing	distance_to_object	stabilize_gaze	Zebra Finch [37]
			adjust_pulse	Hipposiderid Bat [46]
				Big Brown Bat [44, 32]
		altitude	adjust_pulse	Little Brown Bat [41]
		gap_size	adjust_beam_aim	Big Brown Bat [44, 45]
		stationary_object distance_to_object	modify_saccades	Blowfly [8]
		moving_object	change_sensor	Greater spear-nosed Short-tailed fruit Bat [42]
obtain_food	distance_flown	image_motion	return_to_food	Honeybee [35]
	detect_prey	prey_present	maintain_CATD	Big Brown Bat [52]
evade_ predator	detect_predator	predator_present	Not Defined	Greater spear-nosed Short-tailed fruit Bat [42]
track_mate	detect_mate	mate_present	appear_stationary	Hoverfly [28]
center_flight	detect_walls	lateral_image_motion	balance_lateral _motion	Budgerigar[38] Honeybee[43] Blowfly [8]

Table 3.3: Motor schemas utilized to perform a specific behavior with the corresponding percepts.

ter localization and these two adjustments provided time to collect information about the objects to facilitate avoidance.

In [43] the experimentation wasn't intended to showcase the avoidance ability of the honeybees, but rather their ability to choose a flower by determining its distance from their location. Just by the nature of the experimental setup, the honeybees were required to alter their flight paths to avoid the other flowers and arrive at the correct flower with the food reward.

3.5.1.2 Motor Schema: turn_brake or turn_speed

Through flight experiments with the locust, Robertson determined there was always a yaw torque reaction to an obstacle with the addition of either an increase, or decrease in speed. Interestingly, the direction of the turn was not dependent on the side of the animal the obstacle approached. The turn combined with a decrease in speed was seen in response to objects detected late. When objects were detected early the insect increased its speed to power through the avoidance maneuver and maintain its altitude [36].

3.5.1.3 Motor Schema: maintain_angular_velocity

Honeybees reduce their speed when coming in for a landing not by measuring their actual velocity, but by maintaining the velocity of the image of their landing zone as the distance to it decreases. In this way, they ensure their true flight velocity is nearly zero when they land [28].

3.5.1.4 Motor Schema: stabilize_gaze

As described previously, to separate two types of optic flow the zebra finch uses a strategy to stabilize its gaze during flight. This stabilization allows it to extract the rotational optic flow and use only the translational information to estimate distance. The finch achieves the stabilization by alternating fast shifts of its gaze through rotational head

movements with periods of minimal head movement [37].

3.5.1.5 Motor Schema: adjust_pulse

When detecting objects in the flight path the hipposiderid bat will increase the number of pulses it emits in a group by decreasing the duration of the pulse and the interval. The larger the size of the obstacles the sooner the bat will make these adaptations to its detection [46]. To avoid an overlap between the pulses sent and the echoes received the big brown bat emits a shorter sound with a greater rate of repetitions. A decrease in their flight speed also increases the number of pulses they could emit over meters traveled to improve the detection of objects in a cluttered environment [44]. As the big brown bat approached a gap between obstacles in experiments done by Sandig it increased the number of pulses emitted in a group. As the gap size decreased, so did the duration of the pulse while the pulses per group increased. The authors in [32] believe this increase in frequency and decrease in duration improved the accuracy of the target localization for the big brown bat [32]. The little brown bat adjusts its pulse by increasing the number it emits to better localize the landing zone when attempting to land [41].

3.5.1.6 Motor Schema: adjust_beam_aim

When confronted with a cluttered environment the big brown bat sequentially scans by adjusting its gaze to change the direction and distance of the beam of its sonar. In the experiments conducted by [45] the big brown bats adjusted their beam aim between the sides of the gap in the netting eventually concentrating on the prey beyond the netting once they were within a short distance from traversing the gap. This technique improved the target localization and selection for both the gap and the prey. Additionally, Falk noted that when the big brown bat enters the final state of its pursuit of prey it begins to make shallower turns, which also causes an adjustment to the aim of the sonar beam [44].

3.5.1.7 Motor Schema: modify_saccades

The number, direction, and size of saccades a blowfly performs is dependent on the amount of clutter in the environment. The actual movement resembles the banking seen by an airplane when making a turning maneuver where the blowfly is actively controlling the drift to extract distance information. This turn produces movement in three dimensions: yaw, pitch, and roll. Clutter in the environment also prompts a decrease in translational velocity. Interestingly, the decrease does not happen before the blowfly turns, but rather during and after navigation of the turn [8].

3.5.1.8 Motor Schema: change_sensor

The greater spear-nosed bat and short-tailed fruit bat use vision to passively detect predators during rest. Use of vision allows them to conserve their energy and begin to use their active sonar only once a moving predator has been detected in their environment. With the use of their sonar, they are able to accurately locate the prey in order to evade [42].

3.5.1.9 Motor Schema: return_to_food

The honeybee understands and translates the distance it travels to a food source linearly. Researchers believe this makes the encoding to pass along the information to its hivemates in the form of a waggle dance simpler. Using information derived from optic flow the honeybees will fly the distance communicated by their hivemate to reach the food source [35].

3.5.1.10 Motor Schema: maintain_CATD

In order to capture prey that is attempting to evade its predator by making unpredictable movements the big brown bat uses a constant absolute target direction (CATD) strategy to maintain a pursuit trajectory. This approach is ideal because it minimizes the time it takes

the big brown bat to intercept its prey. It accomplishes this by keeping its head locked onto its target once it is in pursuit of the prey even though the direction of flight may change [52].

3.5.1.11 Motor Schema: appear_stationary

Because hoverflies use optic flow to perceive information from the environment, the male hoverfly is able to use this to his advantage when tracking a female for mating purposes. To stay undetected, the male shadows the female. His movements make him appear as a stationary object in the female's environment while she is in motion. Once the female lands, the male flies quickly to her for mating [28].

3.5.1.12 Motor Schema: balance_lateral_motion

Budgerigars prefer centered flight and make use of the lateral portion of optic flow information by keeping the image motion balanced. When the flow becomes unbalanced they veer away from the higher flow with the intent of becoming centered again [38]. Additionally, honeybees prefer to fly in the center of their environment and make adjustments through the optic flow information they receive to keep themselves centered [28]. This same phenomenon is seen in the blowfly where they also prefer to fly in the center of their environment. When obstacles are present, the blowfly maintains a fairly narrow S-shaped flight path as close to the center as it is able [8].

3.6 Observations

During the review of the twenty-three papers in the ethological literature the following four observations emerged: perception through vision is relied on when enough light is present while sonar information is used in darkness, information from one sensor is dominant, adaptive sensing is a valuable strategy, and reduction in speed is a consistent part of the motor response to obstacles in the flight trajectory.

Information perceived from vision sensors is relied upon in lighted scenarios while sonar is dominant for perception in darkness. For all the species surveyed, regardless of whether it was a bird, insect, or bat, the flying animal used information sensed through vision when enough light was available. Conversely, when the articles discussed flight in darkness, the species of birds and bats reviewed relied on the information collected through the use of sonar during flight. Through obstacle avoidance experiments conducted with the greater spear-nosed and short-tailed fruit bats Chase showed their reliance on vision during daylight. Additionally, she hypothesized the importance of vision in recognizing landmarks when navigating to feeding sites due to the distance limitations of sonar [42]. Both the cave swiftlet and oil bird roost in caves where no light penetrates. Because they cannot utilize their vision to sense the cave walls, the ceiling, or other flying animals in the vicinity their use of sonar-like calls is necessary for collision-free flight to and from their nests [51], [50].

Even when multiple sensors are available, the information from on sensor is dominant. Of the twenty-three papers surveyed six discussed the use of both passive and active sensing. In all cases, only information from one sensor was used to make collision-avoidance decisions while the information from the other sensor was discounted. For example, [39] discussed the little brown bat using vision during lighted experiments. Sonar calls were still noted and would have provided information about stationary objects in the bats' flight path; however, the bats still collided with the object. The researchers concluded the bats chose to ignore the contradictory information provided from their sonar and rely solely on their vision for perception. McGuire noted the little brown bat adjusted its acoustic call structure when light was present concluding the animal chose to rely on its vision in a lighted scenario even though it had the option to use sonar to gain more information about the environment [40].

Adaptive sensing is a valuable strategy in flying animals to improve, or increase, the

information they can perceive. The zebra finch stabilizes its gaze to separate rotational from translational optic flow [37]. Increasing the optic flow information perceived by adjusting the number of saccades made in a cluttered environment helps the blowfly gather information about an object it is approaching [8]. Additionally, five of the six named bat species made changes to their sonar call structure when objects were present in their environment [32, 41, 42, 44, 45, 46]. Without these adaptations it is possible these flying animals would not have the information they needed to avoid collisions.

Changing speed was consistently seen in response to objects in the flight path. There were fifteen species named in the papers surveyed, and five of the animals reduced their flight speed when the environment became cluttered: pigeon, zebra finch, honeybee, blowfly, and big brown bat. More specifically, during experiments with the big brown bat Falk noted a reduction in speed from 3.01 m/s to 2.49 m/s when flying in a simulated forest versus an open room [44]. This same species was studied in [32] where approximately a 1 m/s reduction in speed was recorded when the size of the space between obstacles in the environment was 40 to 50 cm. As the gap size was reduced at and below the average wingspan of 30 cm a "more prominent" reduction in flight speed occurred. In the case of the pigeon, the average flight speed of trials without obstacles was 6.95 +/- 0.64 m/s and reduced to 3.86 +/- 0.52 m/s when obstacles were introduced [6]. For the other species, a reduction in speed was mentioned, but no concrete measurements were provided. Ten of the experiments were conducted in simulated environments with the exception of the cave swiftlet [50], oil bird [51], and little brown bat [39, 40, 41], which were all observed in their natural habitats. The other animals were all flight tested in empty rooms where their recorded flight speeds were slower than typical speeds seen in the wild.

3.7 Summary

Through a review of the twenty-three papers from the ethological literature on obstacle avoidance in flying animals five primitive behaviors were identified to provide collision-free flight in unknown and restricted maneuverability environments. Schema theory was used to frame the discussion and decompose the primitive behaviors into the building blocks shown in Figure **??**. Four observations on obstacle avoidance in flying animals were discovered: sensing done by vision in lighted scenarios and sonar in darkness, one sensor always being dominant, adaptive sensing playing a critical role, and reducing speed being a consistent response to objects in the flight path. These four observations were supported by work currently being done in robotics. The work discussed in this dissertation implements a behavior inspired by these insights for autonomous, reactive control of a SUAS in a restricted maneuverability environment. Following the second insight, the perceptual schema relies on input from a vision sensor. The novel APF design was informed by the motor schemas identified and discussed in the ethological literature review. The output vector of the APF provides magnitude and direction. The magnitude profile of the attractive field increases as the platform comes into alignment with the gap, which correlates to the last insight. Details of control rules derived from this review also used in the design of the gap-aiming behavior are discussed in the next chapter.

4. APPROACH

The gap-aiming behavior inspired by flying animals and implemented on a small unmanned quadrotor in this work was designed from three control rules observed in the ethological literature. To determine the current state of the research on reactive control for obstacle avoidance with unmanned aerial systems, a review of the literature was conducted and findings discussed in Chapter 2. Additionally, a review of the ethological literature was conducted to study obstacle avoidance in flying animals for application to SUAS and the details of this review were discussed in Chapter 3. The gap-aiming behavior derived from the study provided a basis for the primary research question posed in Chapter 1. The three control rules used to design the gap-aiming behavior are discussed in detail in Section 4.1 below. The behavior was implemented following a behavior-based robotics approach detailed in Section 4.2. The gap-aiming behavior implementation was tested through simulation to determine the best perceptual schema approach from three possible options: *detect_closest_gap*, *detect_largest_gap*, and *detect_all_gaps*. Following the successful simulation, a proof-of-concept was implemented and tested on a 3D Robotics Solo quadrotor in a restricted maneuverability scenario. The environment and the metrics used to create it are described in detail in Section 6.3.1.

4.1 Control Rules for SUAS Derived from Flying Animals

Concentrating on the avoid_object behavior, the motor schemas discussed in Section 3.5 were aim_gap_center, turn_brake or turn_speed, maintain_angular_velocity, stabilize_gaze, adjust_pulse, adjust_beam_aim, modify_saccades, change_sensor, return_to_food, maintain_CATD, appear_stationary, and balance_lateral_motion. The first two of these motor schemas were the output action of the detect_object perceptual schema. While the actual physical movement is of interest, it is also important to understand when and how

the flying animals choose to perform the movement in order to translate the animal behavior to control of a SUAS. From the ethological literature review provided in Chapter 3, three rules for control of a SUAS are suggested.

First, an appropriate distance to begin maneuvering around an object in the flight path appears to be approximately 1.5 meters. In the literature, the pigeon adjusts its flight path approximately 1.5 meters before colliding with an object [6] and nearly the same is seen with the big brown bat [32]. The bat begins effecting an avoidance maneuver 2.0 to 1.5 meters before it would collide with the object. The distance when the pigeon and big brown bat begin maneuvering is not influenced by the size and number of obstacles in the environment, which is defined as the severity of obstacles in [9]. Additionally, this distance does not rely on the size of the gap between obstacles. What is similar between the two species is the scale of the region where they are able to navigate, which is defined in [9] as the relationship between the size of the agent and the environment. Specifically, these two species can navigate in a restricted maneuverability region where the environment is less than two times the size of the agent and the buffer distance required. Additionally, the environment is larger than the size of the agent plus the buffer. Together, the agent size and the buffer are referred to as the effective agent size. This is described as:

$$2 * (\text{effective agent size}) > \text{environment} > \text{effective agent size} \tag{4.1}$$

The pigeons never flew closer than 4.3cm to any obstacle and, since they navigate through 30cm-wide gaps with their wings tucked, the animal measurement is their 10cm torso. Using Equation 4.1, the scale of the region is calculated for these pigeons during this experiment as: 2*(10cm + 4.3cm + 4.3cm) >30cm <(10cm + 4.3cm + 4.3cm).

For the big brown bat, the 100% collision-free flights were performed when the gap size between obstacles was 40cm. This animal has a wingspan of 30cm and is not de-

scribed as requiring any buffer distance. The scale of the region computes as: 2*30cm >40cm <30cm.

Second, maneuvering through the largest gap between objects is preferred. Both pigeons and starlings favor the largest visual gap during flight [6], [7]. Through flight experiments with pigeons, [6] determined the birds preferred to maneuver through the largest gap versus the closest when at higher flight speeds. Starlings also aim adjustments in their flight path to the largest gap to avoid the risk of a collision and therefore potential injury [7]. These birds make this tradeoff for the largest gap at the expense of maintaining a nearly straight flight path. This allows them to maintain higher flight speeds while still navigating collision-free. This strategy was employed in simulation and physical experiments on a ground vehicle with successful collision-free results in a simplified test scenario with seven static obstacles and a goal in front of the vehicle. They followed this with an experiment using four dynamic obstacles the vehicle successfully passed over 60 meters [57].

Third, remaining centered in a flight corridor and when traversing between obstacles is preferable. Pigeons, honeybees, and blowflies all showed a preference for centering their flight path. In initial testing, [6] showed the pigeon flew in the center of an unobstructed corridor. When objects were introduced, the pigeons deviated from their flight path to avoid the object, but returned to the center of the corridor when able. The flight path with obstacles present was measured to be only 8% longer than a straight path through the unobstructed corridor. In [35], Srinivasan noted the honeybee flies through the center of an open window, and in the middle of a tunnel during experiments. The blowfly chose a flight path in the center of experimental tunnels. When objects were present, the blowfly performed avoidance maneuvers to create a narrow S-shaped flight path as close to the center as possible while remaining collision-free [8].

4.2 Behavior-Based Robotics

To realize the gap-aiming behavior derived from the observed control rules discussed in Section 4.1, a behavior-based approach to robotics is used. In behavior-based robotics, behaviors are the basic building blocks which make up an intelligent agent and all action in a reactive paradigm is done through these behaviors. Because the reactive paradigm does not have a planning component, a task is accomplished by the sense and act primitives, which make up a behavior [1]. A *behavior* accepts inputs from one or more sensors, processes the sensing data via a *perceptual schema* to produce a *percept* which produces a motor action via a *motor schema*. Schema theory was previously discussed in Chapter 2 to frame the literature review of reactive control for obstacle avoidance in SUAS and in Chapter 3 for the ethological literature review with an illustration in Figure **??**. The following subsections briefly describe the perceptual schema and motor schema building blocks to be used in designing the gap-aiming behavior. An in-depth explanation of the implementation details is provided in Chapter 5.

The advantage of using this behavior-based robotics approach is threefold. First, the primitive building blocks of a behavior are exchangeable because they are independent of each other. In this way, the motor schema is not reliant on the specific perceptual schema implemented in this work. A more sophisticated perceptual schema could be introduced in the future, which provides this motor schema implementation with the required percepts. Second, the APF implementation of the motor schema could be tuned with knowledge of the dynamics of the SUAS. Finally, additional behaviors can be added to the system. Because more than one of these behaviors may be active simultaneously a procedure for determining the ultimate motor action must be implemented whether it is the output of a single behavior, or combination of behaviors. Additionally, it is important to note that an obstacle avoidance behavior would not be necessary in addition to the gap-aiming behavior

designed in this work because if no gaps exist in the environment, then the APF would produce no motor actions. In other words, with only the gap-aiming behavior implemented the lack of a gap in the FOV for the quadrotor used in the proof-of-concept demonstration would cause the platform to hover.

4.2.1 Perceptual Schema

A perceptual schema is responsible for creating the necessary information from the sensor input required by the motor schema to produce the desired action. From a visually collected image, the gap-aiming behavior relies on the perceptual schema to detect one, or more unobstructed areas available in the FOV for SUAS flight. Because multiple gaps may exist within the image and the ethological literature was unclear whether flying animals were reacting to the closest, largest, or all the gaps in the FOV, there are three approaches available for creating the perceptual schema in the gap-aiming behavior. The first two approaches follow a winner-take-all strategy where the perceptual schema identifies either the closest, or the largest gap in the FOV. In the third approach, the perceptual schema detects all of the gaps in the FOV. Following Arkin's method for robot navigation [10], the percepts are used by the motor schema to produce velocity and steering commands to move the SUAS.

4.2.2 Motor Schema

Frequently implemented forms of behavior-based reactive control are subsumption, and artificial potential fields (APF) [1]. The latter is a widely used method to control robot behavior and is the method employed in this work. The artificial potential fields methodology was originally developed and applied to manipulators and mobile robots by Oussama Khatib [58] in 1985. The implementation made use of an attractive potential field for the goal(s) and a repulsive potential field for the obstacle(s). A vector is used to define both the direction and magnitude of the force exerted on the robot at any one

point in the field. When multiple instantiations of the motor schema are exerting a force in the same location, then vector summation is used to create one resultant vector. In addition to the attractive and repulsive fields used in [58] there are three other primitive fields: uniform, perpendicular, and tangential. These five primitive fields are illustrated in Figure 4.1, which is taken from [1] where a detailed description of each of the fields can be found. The collection of arrows denotes the region in space where the potential field would exert a force on the robot. Individually, the orientation of the arrow shows the direction of the force and the length of the vector defines the magnitude. The magnitude can be just a constant value, or the profile could have a linear, or exponential drop off. However, any magnitude profile could be tuned to create the desired results from the behavior. For example, Connolly made use of harmonic functions to create the artificial potential field used in their application [59] while Vadakkepat developed a genetic algorithm to adjust the constant value used to compute the force [60].

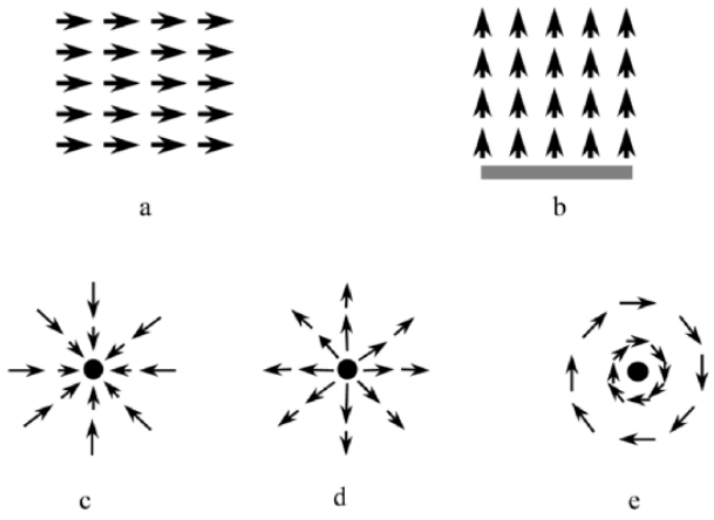

Figure 4.1: Illustration of five primitive potential fields. Reprinted from [1].

A potential field is defined as the scalar U, which is the combination of all fields in the environment. In the case that both a repulsive and an attractive field are present, then Equation 4.2 defines the scalar potential field where U_{rep} is the repulsive field and U_{att} is the attractive field.

$$(\mathrm{U}) = \mathrm{U}_{\mathrm{rep}} + \mathrm{U}_{\mathrm{att}} \tag{4.2}$$

In the case of reactive control, the force exerted on the robot is only calculated at it's current position in the potential field. For visualization purposes we can compute all of the vectors in the force field as the negative gradients of their respective potential field, as illustrated in Equation 4.3.

$$(\mathrm{F}) = -\nabla \mathrm{U}_{\mathrm{rep}} + -\nabla \mathrm{U}_{\mathrm{att}} \tag{4.3}$$

As an example, if the force vectors of a repulsive field with a linear dropoff magnitude profile and two attractive fields with a conical and a quadratic magnitude profile were combined they would resemble Figure 4.2. This illustration was taken from [2] and is a three dimensional representation of the overall potential when combining these three fields.

4.3 Bio-inspired APF Implementation

With inspiration from flying animals, this work implements a gap-aiming behavior to implicitly avoid obstacles by using a motor schema implemented with an APF to create the actions required to aim to the center of the gap. This novel bio-inspired APF implementation makes use of both a selective attractive and tangential field. The selective attractive field is used to attract the SUAS to the gap and the addition of the tangential field aligns the SUAS for flight straight through the gap. Because the behavior is not explicitly

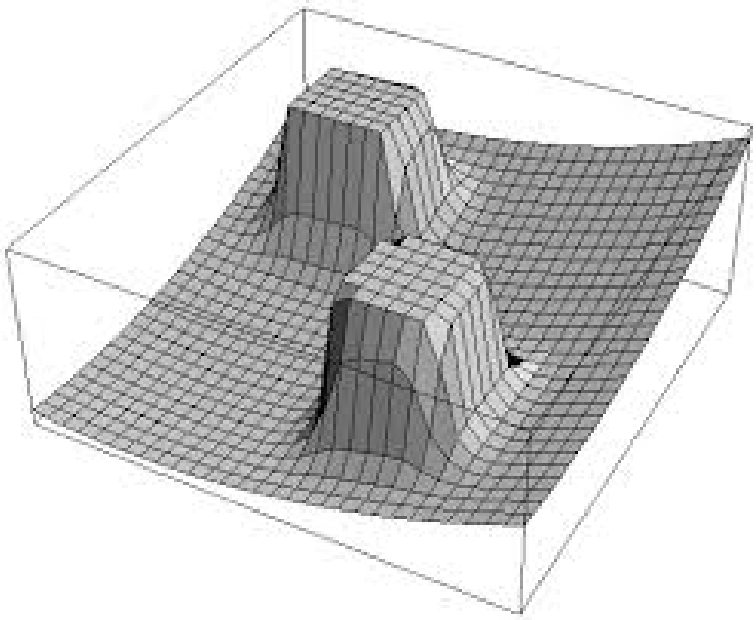

Figure 4.2: 3D illustration of the overall field used in [2]. Reprinted from [2]

avoiding obstacles like the typical APF implementation no repulsive field is used in the implementation.

4.4 Metrics to Quantify the Flight Environment

The approach to evaluate the gap-aiming behavior uses a subset of metrics taken from disaster robotics [9] to quantify the experimental flight environment. The subset of metrics was selected to reflect both the interior of a building damaged by a disaster and the experimental environments where flying animals were observed in the review of the ethological literature from Chapter 3. As discussed in Section 2.4, current implementations were not tested in highly confined experimental environments representative of what might be encountered in the interior of a building following a natural disaster. Additionally, there were no consistent metrics used to define the experimental environment, or to assess the success of an obstacle avoidance implementation.

The subset of metrics used comes from a comprehensive suite of metrics provided in

Table 4.1: Three attributes used to describe a region of the operational environment and their categories.

	ATTRIBUTES		
	Non-navigational Constraints	**Scale of the Region**	**Traversability of the Region**
CATEGORIES	Meeting Survivability	Granular	Tortuosity
	Sensing	Restricted Maneuverability	Verticality
	Maintainability Requirements	Habitable	Surface Properties
	Managing Unintended Consequences	Exterior	Severity of Obstacles
			Accessibility Elements

[9]. The comprehensive suite of metrics consists of three attributes to describe a region of the operational environment: non-navigational constraints, scale of the region, and the traversability of the region. The attributes all contain multiple categories and are shown in Table 4.1. The details of the categories contained in the comprehensive suite of metrics can be found in [9].

This work uses a subset of these metrics to define the experimental environment described in detail in Section 6.3.1. The scale of the region attribute and the tortuosity category of the traversability attribute are used. The scale of the region is used to define the relationship between the size of the environment and the SUAS used for the field experiments. The scale of the region for the field tests was designed to be restricted maneuverability to demonstrate the gap-aiming behavior can produce autonomous, collision-free flight in an environment comparable to that used in flying animal observations. Additionally, the ability to move through the environment is the traversability of the region. The tortuosity category of this attribute is a measure of the number of turns the SUAS is re-

quired to make over the distance travelled. Because the motivation for this research is an indoor disaster environment, a measurement of 0.6 for the tortuosity taken from Michael's work surveying the interior of a building at Tohoku University damaged after the 2011 earthquake in Japan is used [61]. This subset of quantitative metrics are described in detail for the proof-of-concept environment designed for the field experiments in Section 6.3.1.

4.5 Visual Servoing

A behavior-based robotics approach was taken in this work to implement a gap-aiming behavior inspired by flying-animals, which is related to image-based visual servo control (IBVS), a type of visual servoing. The gap-aiming behavior uses input from a visual sensor and produces motor actions through an APF to aim a small unmanned quadrotor to the center of a gap in the environment. As defined in the Springer Handbook of Robotics, visual servoing "uses computer vision data in the servo loop to control the motion of a robot" [62]. Visual servoing requires tracking of two dimensional features or three dimensional models, or relies on motion analysis in an image sequence [63]. Implementations of this visual servoing technique can be categorized as IBVS, pose-based visual servo control (PBVS), or an advanced approach.

At least three different implementations of image-based visual servo control exist on SUAS and are discussed below. In [64] a non-linear controller with an integral backstepping approach for a Pelican quadrotor was designed, which took translational velocity input using four visual features to track a target. To grasp an object with a robotic arm mounted on a multirotor, Kim uses image moments as input to a passivity-based adaptive controller [65]. Lee used the IBVS control by applying a nonlinear model predictive controller that combined the dynamics of a fixed-wing platform and camera geometry [66].

There are both similarities and differences between the previously discussed approaches to autonomous collision-free flight on a SUAS and the one taken in this work. A behavior-

based robotics approach used in this work is related to IBVS control because the perceptual schema makes use of image moments, namely the centroid of a blob. Additionally, the novel APF implemented in this work produces the vector to adjust the flight path of the SUAS towards this centroid providing high-level velocity control. This high-level control differs from the low-level control provided by the previously discussed implementations. Those controllers provided low-level attitude control and were tuned to the specific vehicles used for experimentation. In contrast, the gap-aiming behavior implemented in this work does not rely on the dynamics of the vehicle and so it is extensible to other rotorcraft.

4.6 Summary

Because animals successfully fly collision-free in environments with closely spaced obstacles, a review of the ethological literature was performed to determine the motor schemas they use to avoid obstacles. During the review, three rules were identified: the appropriate distance to begin maneuvers, the direction to adjust the flight path, and the role of centered flight. The combination of these control rules to create autonomous collision-free flight on a SUAS resulted in the design of a gap-aiming behavior. This behavior was implemented using a behavior-based robotics approach. The perceptual schemas and motor schema used are described in detail in the following chapter. Simulations were completed to determine the best perceptual schema approach to use for the proof-of-concept implementation and testing on a 3DRobotics Solo quadrotor in a restricted maneuverability environment. The method, metrics, and experimental environment used are described in detail in Chapter 6.

5. IMPLEMENTATION[1]

This chapter describes the implementation of the Matlab®simulation for Study 1 and the proof-of-concept demonstration. It details the hardware and software used to create the simulation for Study 1, as well as the quadrotor platform and visual sensor used for the proof-of-concept demonstration. Additionally, the implementation of the perceptual schemas tested in Study 1, and motor schema for the gap-aiming behavior are discussed in detail in this chapter.

5.1 Software and Hardware Description

Described in detail in the following chapter, Study 1 was designed and conducted via simulation to test two hypotheses about the primary research question [67]. The software used to implement the motor schema via an APF and the three perceptual schema approaches in simulation was Matlab 9.0 Release R2016a. The simulation was run on a MacBook Pro using OS X El Capitan version 10.11.6. The laptop contains a 2.9 GHz Intel Core i7 processor, 8 GB of 1600 MHz DDR3 RAM, and an Intel HD Graphics 4000 card.

The proof-of-concept was implemented on a 3DRobotics Solo quadrotor platform. This quadrotor is 46 cm from motor to motor and 56 cm in width with blades attached, weighs 1.5 kg carrying no payload, has a payload capacity of 800 g, and a reported maximum speed of 89 km/hr [68]. It runs the APM autopilot software on a Pixhawk 2 [69], contains an iMX6 companion computer with Yocto Linux, and carried a GoPro Hero4 Silver on a gimbal during proof-of-concept testing. The GoPro weighs 84 g and measures 41 mm high by 59 mm wide by 29.6 mm deep. The settings for the camera are shown in Table 5.1.

[1] ©2016 IEEE. Portions of this chapter reprinted with permission from Sarmiento and Murphy, "Artificial potential field implementation of flying animal gap-aiming behavior in 3d, IEEE International Symposium on Safety, Security, and Rescue Robotics (SSRR), 2016

Table 5.1: GoPro Hero4 Silver camera settings for proof-of-concept testing

Resolution	1080p
Field of View	Medium
Low Light	Off
White Balance	Auto
ISO	400
Protune	On

5.2 Gap-Aiming Behavior

A primitive gap-aiming behavior used to produce collision-free flight was extracted from a review of the ethological literature. To implement this gap-aiming behavior seen in flying animals for a SUAS a behavior-based robotics approach based on Arkin's work [10] was taken. The primitive gap-aiming behavior shown in Figure 5.1 feeds a visually-collected image into the *detect_gap* perceptual schema, which provides percepts to the *aim_gap_center* motor schema. This motor schema is implemented through the use of an artificial potential field and is described in detail in Subsection 5.2.2.

Because the ethological literature was unclear whether flying animals were reacting to the closest, largest, or all of the gaps in the FOV, three perceptual schema approaches were investigated in simulation: *detect_closest_gap*, *detect_largest_gap*, and *detect_all_gaps*. The first two illustrated in Figure 5.1a are winner-take-all approaches, where the perceptual schema selects one gap and provides the corresponding percepts to the motor schema. The third approach shown in Figure 5.1b uses summation to combine the vectors resulting from the multiple instantiations of the motor schema. The perceptual schema approach determined to be the best through evaluation of two hypotheses using two metrics in Study 1 was implemented for the proof-of-concept demonstration.

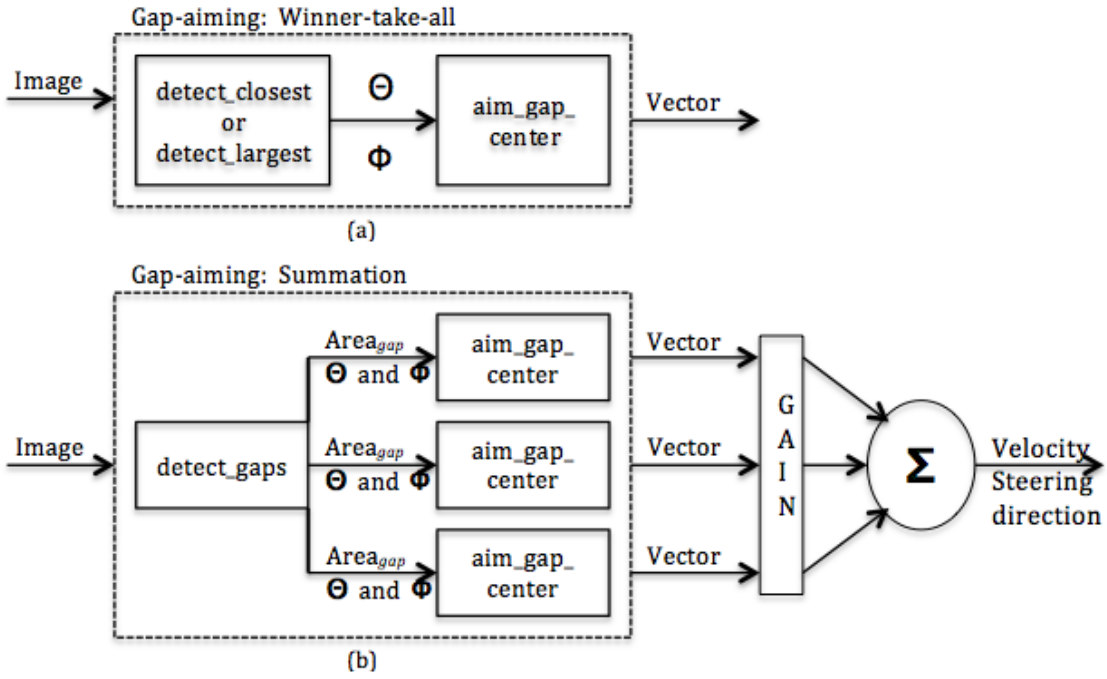

Figure 5.1: (a) Flying animal inspired gap-aiming behavior with Winner-take-all perceptual schema approaches: *detect_closest_gap* and *detect_largest_gap* (b) with summation perceptual schema approach: *detect_all_gaps*

5.2.1 Perceptual Schema Approaches

A perceptual schema is a building block of a primitive behavior, which takes input from one, or more sensors and provides the appropriate percepts to the motor schema. The *aim_gap_center* motor schema expects the perceptual schema to provide information about the unobstructed portions of the flight environment. The two winner-take-all perceptual schema approaches *detect_closest* and *detect_largest* produce two percepts from a single selected gap. In simulation, the two percepts are the angles θ and ϕ calculated in reference to a three-dimensional robot-centric spherical coordinate system because depth was available. This is illustrated in Figure 5.2.

As shown in Figure 5.2, the z-axis is vertical, the x-axis moves left to right, and the

y-axis extends into the environment. The orientation of the x-y-z axes correspond to the default viewpoint in Matlab®. The angle, θ, is a measure of the angle between the center of the gap and the SUAS location in the x-y plane. The angle, ϕ, is a measure of the angle between the center of the gap and the SUAS location in the y-z plane. Traditionally, θ has values from 0° to 360°and ϕ from 0° to 180°. To compute the magnitude for the APF, the values are adjusted to range from -180° to 180°and -90° to 90°, respectively. Any gap not perceivable because it is outside the FOV of the visual sensor results in a magnitude calculation of zero. In the proof-of-concept implementation on the 3DRobotics Solo quadrotor where depth is not available, the percept angles are azimuth and elevation computed from image coordinates in a frame taken from the live video feed of the GoPro Hero4 Silver. This is described in further detail in Section 5.3.

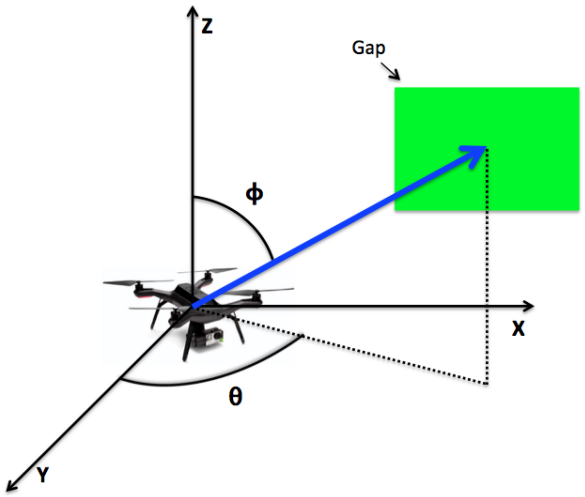

Figure 5.2: Angles θ and ϕ measured by all three perceptual schema approaches

The steps taken by the *detect_closest_gap* perceptual schema used in the Study 1 simulation are outlined in Algorithm 1. From a visually collected image, all of the gaps in

the FOV are identified. For each gap, the θ and ϕ angles are calculated and combined. The combined value is stored and eventually compared against all of the other gap-angle values to select the gap closest to the SUAS. The θ and ϕ percepts are then set to the values pertaining to the selected gap. Following Arkin's method for robot navigation [10], these two percepts are used by the motor schema to calculate velocity and steering commands to produce the desired action of the SUAS.

Algorithm 1 Perceptual Schema: detect_closest_gap

Input: Visually collected image
Output: θ and ϕ of closest gap

```
1: detect all gaps
2: for each gap do
3:     compute θ to gap center
4:     compute φ to gap center
5:     add θ and φ
6:     store combined angle value
7: end for
8: select smallest combined angle
9: set θ and φ to values of selected gap
```

Algorithm 2 outlines the steps taken by the *detect_largest_gap* perceptual schema. From a visually collected image, all of the gaps in the FOV are identified. For each gap, the width and height in image pixels is determined. Using these values the area of the gap is computed and stored. All of the gap area measurements are compared and the largest gap is selected. The θ and ϕ angles for the selected gap are calculated and forwarded as percepts to the *aim_gap_center* motor schema.

Algorithm 3 outlines the steps taken by the *detect_all_gaps* perceptual schema. From a visually collected image, all of the gaps in the FOV are identified. For each gap, the θ and ϕ angles, and the width and height measurements in image pixels are determined. The

Algorithm 2 Perceptual Schema: detect_largest_gap

Input: Visually collected image
Output: θ and ϕ of largest gap

```
1: detect all gaps
2: for each gap do
3:     calculate width in pixels from image
4:     calculate height in pixels from image
5:     compute area from width and height
6:     store area value
7: end for
8: select largest area
9: set θ and φ to values of selected gap
```

width and height measurements are used to compute the area of the gap, $Area_{gap}$. An array of θ, ϕ, and $Area_{gap}$ for all of the gaps is created. A motor schema is instantiated for each gap and its corresponding percepts. Details of the summation of multiple instantiations of the *aim_gap_center* motor schema used to produce the appropriate motor actions is discussed in the following subsection.

Algorithm 3 Perceptual Schema: detect_all_gaps

Input: Visually collected image
Output: θ, ϕ, and area of all gaps

```
1: detect all gaps
2: for each gap do
3:     compute θ to gap center
4:     compute φ to gap center
5:     store θ and φ values
6:     calculate width in pixels from image
7:     calculate height in pixels from image
8:     compute area from width and height
9:     store area value
10: end for
11: output array of θ, φ, and area values of all gaps
```

The gaps detected are considered navigable regions of the environment for the SUAS. This means an assumption is made that there exists a space equal to, or larger than the size of the SUAS with no obstructions in the environment. Additionally, because no depth information is collected the gaps all appear to be the same distance from the SUAS.

5.2.2 Motor Schema: Artificial Potential Fields

Motor schemas take percepts as input and produce an output vector for action through the implementation of an APF. The force exerted on the SUAS at its current position in an APF is a vector with both a magnitude and direction component. The magnitude profile describes how the magnitude value of the vectors change in the APF. This profile could be constant, linear, exponential, or a custom creation.

With inspiration from flying animals, this work implements a gap-aiming behavior to implicitly avoid obstacles by using a motor schema to create the actions required to aim to the center of the gap through the use of APFs. A selective attractive field is used to attract the SUAS to the gap with the addition of a tangential APF to align the SUAS for flight straight through the gap. Because the behavior is not explicitly avoiding obstacles like the typical APF implementation no repulsive field is used.

For the first two approaches where the perceptual schema identifies one gap there is one instantiation of the *aim_gap_center* motor schema with one output vector. For the third approach where multiple gaps are identified the motor schema is instantiated for each gap with its corresponding percepts shown in Figure 5.1b. Because there are multiple instantiations of the motor schema and therefore, multiple output vectors a gain vector is computed to prioritize a gap over others. Equation 5.1 defines the calculation of the gain value for each perceived gap.

$$\text{Gain} = {}^{Area_{\text{gap}}}\!/_{Area_{\text{Image}}} + \left(1 - {}^{(\theta+\phi)}\!/_{90}\right) \tag{5.1}$$

The gain is computed by combining a value for the size of the gap with a value for the closeness. The portion of the gain pertaining to the size is calculated by dividing the area of the gap, $Area_{gap}$, by the area of the overall image in pixels, $Area_{Image}$. The portion of the gain pertaining to the closeness is calculated by adding the θ and ϕ angles previously described, and dividing them by 90. This value is then subtracted from 1. This is the equation of a line with x-intercept of 90 and slope of -1/90.

These two values are combined to calculate the gain for the specified gap. This gain is multiplied by the output vector of the motor schema pertaining to the same gap. This computation is done for each motor schema instantiation at the current SUAS location and the updated output vectors are summed into a resultant vector for action. Figure 5.1b shows the three motor schema instantiations, their vector outputs multiplied by the gain, then fed into the summation with a resultant velocity and steering direction output.

The actions of the motor schema, which aims to the gap center are created through the summation of the force vectors computed at the current SUAS location. Much like the docking motor schema in [70], there are multiple fields exerting a force on the SUAS at a single location. The combination of a selective attractive potential field shown in Figure 5.3a and a tangential potential field shown in Figure 5.3b provide the velocity and steering commands of the motor schema aiming to the gap center. Although the actual flight path of the SUAS would be created by summing the vectors at a single location the entire potential field is shown. Figure 5.3a and b shows the two fields separately with a view of the two-dimensional x-y plane. Additionally, Figure 5.3c shows a side view of the combined fields in three dimensions with one gap present in the environment. The final portion of Figure 5.3d is a three dimensional view image as the SUAS would view the gap when its flight path is aligned with the y-axis. The calculation of the magnitude and direction of the vectors creating the individual potential fields are described in more detail in the following subsections. Again, because the motor schema is aiming to the gap center

to autonomously fly collision-free and not explicitly avoiding obstacles no repulsive field is used in this implementation.

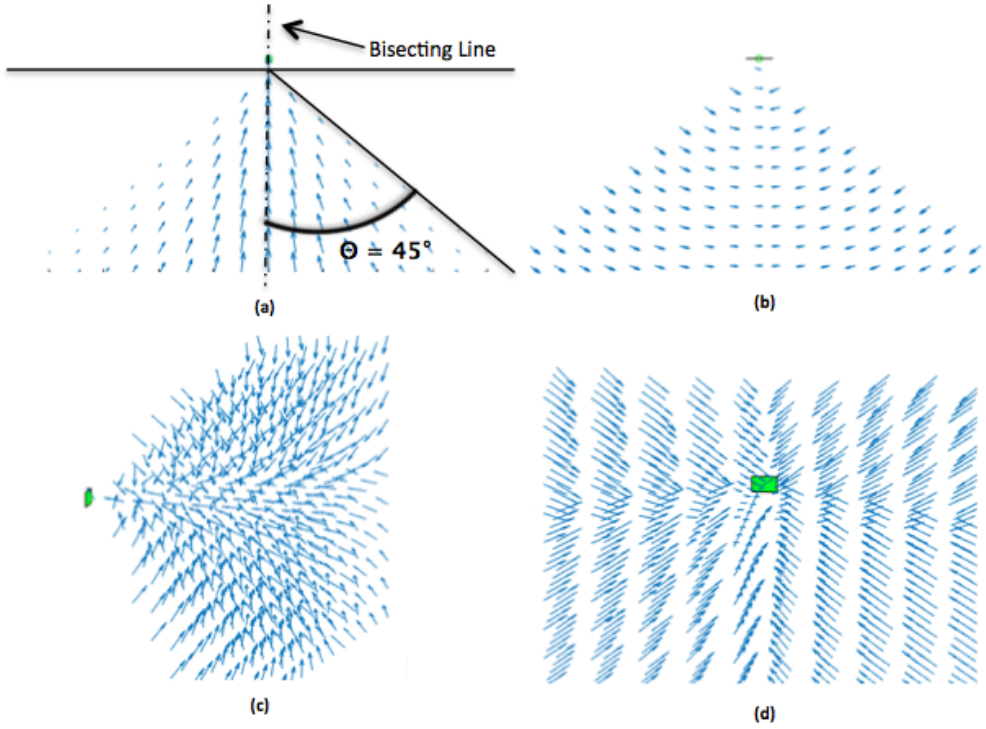

Figure 5.3: (a) Two-dimensional view of the selective attractive field in the x-y plane (b) Two-dimensional view of the tangential field in the x-y plane (c)Three-dimensional side-view showing the combined selective attractive and tangential fields for one perceived gap (d) Three-dimensionsal forward view showing the combined selective attractive and tangential fields for one perceived gap

5.2.3 Selective Attractive Potential Field

The selective attractive potential field is used to attract the SUAS to the center of the gap. The range of the effect of the selective attractive potential field is not a distance value typically seen with the use of APFs. Rather, it is exerting a force on the SUAS whenever the gap is perceivable. The width and height of the perceivable area is deter-

mined by the FOV of the vision sensor used to capture images of the environment. For the Matlab®simulation, 90° is selected as a conservative estimate of this FOV value. This effectively creates an APF in the shape of a right circular cone. It has its vertex at the gap center with its axis parallel to the y-axis and a semi-vertical angle of 45°. For the proof-of-concept demonstration, the true FOV of the vision sensor carried onboard is used.

The magnitude of this field increases linearly as the SUAS approaches the line running parallel to the y-axis that bisects the gap shown in Figure 5.3a. The length of the arrow denotes the magnitude of the vector, which increases as the SUAS approaches the bisecting line. This linear increase is defined in Equation 5.2 where *MaxAngle* is a measure of the addition of the maximum distance in degrees the two angles, θ and ϕ, could be from the bisecting line and still be affected by the field. Figure 5.3a is a view of the x-y plane and shows the maximum measurement of θ_{Max} is equal to 45°for the simulation. The angle ϕ is measured in the y-z plane. The normalized value described previously and shown in Figure 5.2 is used. The addition of θ_{Max} and ϕ_{Max} is *MaxAngle = 90°* in the simulation. When the SUAS falls outside of the influence of the selective attractive field the magnitude of the vector is zero. The vector is directed towards the center of the gap, which is shown in Equation 5.3.

$$\vec{v}_{\text{mag}} = \begin{cases} (\text{MaxAngle} - |\theta| + |\phi|)/\text{MaxAngle} & \text{for } |\theta| \text{ or } |\phi| \leq 45^\circ \\ 0 & \text{for } |\theta| \text{ or } |\phi| > 45^\circ \end{cases} \tag{5.2}$$

$$\vec{v}_{\text{dir}} = \text{direction of gap} \tag{5.3}$$

5.2.4 Tangential Potential Field

The selective tangential field is used to align the SUAS for straight flight through the selected gap. This field affects the SUAS when the gap is perceived by the vision sensor

with the same measurements previously described. The tangential field has a decreasing linear magnitude profile and is shown in Equation 5.4. The vector is rotated 90° towards the line that runs parallel to the y-axis and bisects the gap. The direction of these tangential vectors is denoted in Equation 5.5. The tangential APF for one perceivable gap is shown in Figure 5.3b.

$$\vec{v}_{\text{mag}} = \begin{cases} (|\theta| + |\phi|)/90 & \text{for } |\theta| \text{ and } |\phi| \leq 45^\circ \\ 0 & \text{for } |\theta| \text{ and } |\phi| > 45^\circ \end{cases} \tag{5.4}$$

$$\vec{v}_{\text{dir}} = \pm 90^\circ \text{ toward the bisecting line} \tag{5.5}$$

5.3 Perceptual Schema for Proof-of-Concept Demonstration

A GoPro Hero4 Silver is used as the visual sensor to provide an image to the perceptual schema for processing. A frame is pulled in real-time from the live video feed of the GoPro and sent to the perceptual schema to detect the closest gap in the image. The perceptual schema is responsible for detecting the closest gap in the image provided as input from the visual sensor. It is done through blob detection using OpenCV running onboard the SUAS. Gaps detected are considered navigable regions of the environment for the SUAS. This means an assumption is made that there exists a space equal to, or larger than the size of the SUAS with no obstructions in the environment. Figure 5.4a is a frame pulled from the live video feed of the onboard visual sensor. This frame is turned into a grayscale image as shown in Figure 5.4b, then the panel is separated from the surrounding area and thresholded to create the binary image shown in Figure 5.4c. From this binary image the blobs (gaps) are detected and the closest gap is found.

Closeness is determined by the difference in image coordinates between the center of the image and the center of the gap. The latter is equal to the centroid of the blob. Using

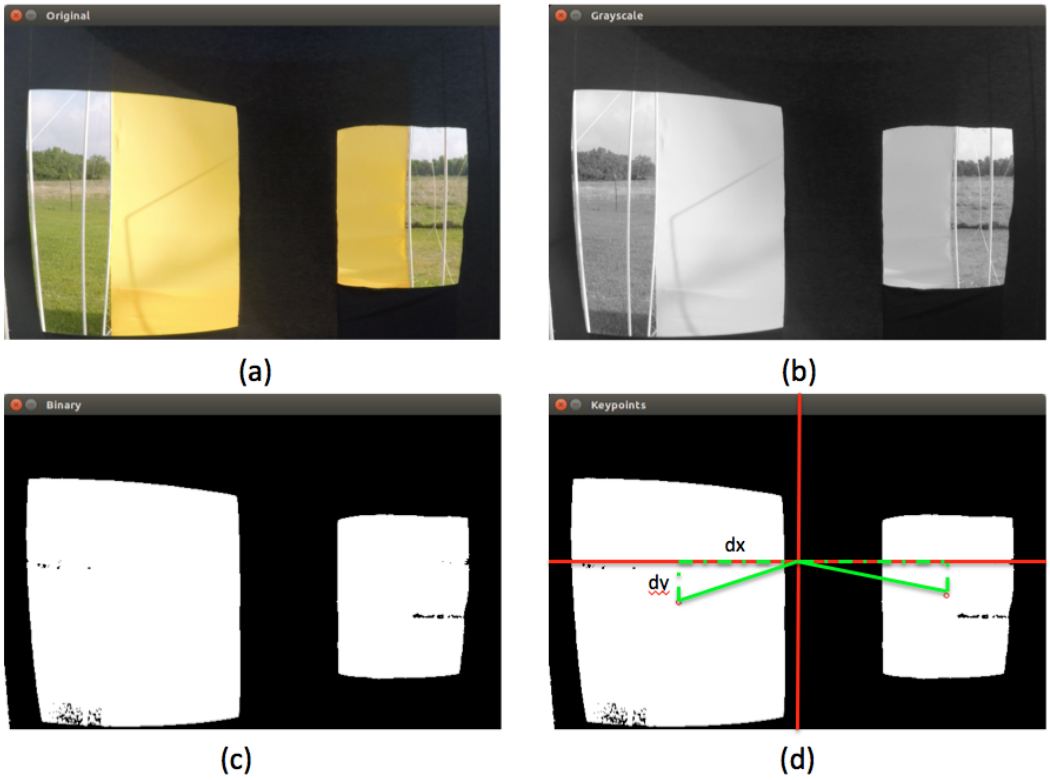

Figure 5.4: (a) Original image taken from live video stream of onboard visual sensor (b) First processing step turns original image to grayscale (c) Thresholding used to separate the panel from the perceived gaps (d) Computation to determine the closed gap for traversal using image coordinates

the Pythagorean Theorem, the shortest hypotenuse is determined to be the closest gap. This computation is shown in Figure 5.4d. From this closest gap, the perceptual schema provides the angle percepts the *aim_gap_center* motor schema expects. As discussed previously, the θ and ϕ angles must be approximated because the images are processed in two dimensions.

With knowledge of the center of closest gap, the center of the image, and information about the field of view of the visual sensor, θ, is calculated as the angle between the center of the image and the center of the gap in the x-direction. It is a measure of how far to the left, or right of the center of the image the gap resides. The angle ϕ, is calculated as

the angle between the center of the image and the center of the gap in the y-direction. It is a measure of how far above, or below the center of the image the gap resides. Given the measurements in Figure 5.5 angle θ is approximated as -22.7° using Equation 5.6 and angle ϕ is approximated as 5.0° using Equation 5.7.

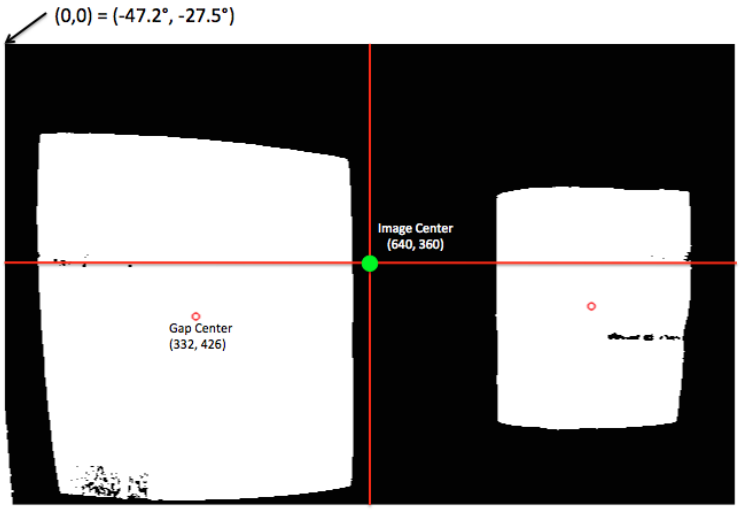

Figure 5.5: Angles θ and ϕ measured by the perceptual schema

$$\theta = \left({}^{HorizontalFOV}/_{ImageWidth}\right) * \Delta x \tag{5.6}$$

$$\phi = \left({}^{VerticalFOV}/_{ImageHeight}\right) * \Delta y \tag{5.7}$$

5.4 Summary

The implementation details of the gap-aiming behavior in simulation and for the proof-of-concept demonstration were described in this chapter. The three perceptual schema approaches tested via simulation, the one utilized in the proof-of-concept demonstration,

and the motor schema implemented with an artificial potential field were described. Also, the hardware and software used for the simulation, and the quadrotor platform and visual sensor used for the proof-of-concept demonstration were identified.

6. EXPERIMENTAL METHODS, DESIGN, AND RESULTS[1]

To answer the primary research question introduced in Section 1.1, which is derived from observations of flying animals discussed in Section 4.1, one study was designed to test two hypotheses in simulation. The study and hypotheses tested are described in Section 6.1. Additionally, the gap-aiming behavior was implemented on a 3DRobotics Solo quadrotor and tested in two sets of field experiments. The purpose of this proof-of-concept demonstration and the metrics used to analyze the flights are outlined in Section 6.3 of this chapter.

6.1 Study 1: Perceptual Schema Approach

Because biological studies are unclear whether flying animals react to the closest gap, largest gap, or all of the gaps in their environment this study was designed to determine the best perceptual schema approach to use with a gap-aiming behavior. This study tests two hypotheses detailed below and the results are presented in Section 6.2.

Hypothesis 1: Using a winner-take-all approach to perceive a gap in the environment for action will result in a smoother path.

A simulation was designed in Matlab® to determine the correct perceptual schema approach to use to elicit the best performance from the gap-aiming behavior. The *aim_gap_center* motor schema was implemented through the use of an APF described in detail in Chapter 5. The three perceptual schema approaches also described in Chapter 5 were tested over one hundred and twenty simulation runs and compared quantitatively through the use of the smoothness metric to test Hypothesis 1. These three perceptual schema approaches are: *detect_closest_gap*, *detect_largest_gap*, and *detect_all_gaps*.

[1] ©2016 IEEE. Portions of this chapter reprinted with permission from Sarmiento and Murphy, "Artificial potential field implementation of flying animal gap-aiming behavior in 3d,? IEEE International Symposium on Safety, Security, and Rescue Robotics (SSRR), 2016

Table 6.1: Description of variables to be varied and measured in Study 1 to test Hypothesis 1 and Hypothesis 2

TYPE OF VARIABLE	VARIABLE	VALUE
Independent	Perceptual Schema	Closest, Largest, or All Gaps
	Gaps	Beginning with 1 in Environment 1 and increasing to 10 in Environment 10
	Starting Location	Random location in each of the 4 quadrants for 10 environments
Dependent	Smoothness	Square of the change in path curvature with respect to time
	Path Length	Difference in length straight path vs. actual path (%)

For each of the three perceptual schema approaches forty simulations are run in Matlab® for a total of one hundred and twenty runs. Each of the three sets of forty simulations are comprised of ten environments with the number of gaps ranging from one to ten. The first environment has one gap, the second has two, and the pattern continues up to ten gaps in the tenth environment. In each of these ten environments there are four starting locations with one corresponding to each quadrant found in a rectangular coordinate system. Those quadrants are in the x-z plane shown in Figure 5.2. The location and size of the gap(s), and the starting locations of the SUAS are randomly selected with the use of the rand() function in Matlab® for uniformly distributed random numbers. The smoothness metric, detailed below, is collected and used to compare the simulation runs. Table 6.1 identifies the independent and dependent variables described and used to test Hypothesis 1.

6.1.1 Smoothness

A smooth path is important for SUAS operation to potentially reduce energy expenditure and produce time savings. The smoothness of a trajectory was defined by Rosenblatt [71] as the square of the change in a vehicle path's curvature, κ, with respect to time, then integrated along the entire path and finally normalized by the time. This is shown in Equa-

tion 6.1, where *l* is the length of the path and *s* is the arc length. Arc length is a measure of the length of the 3-dimensional path and is computed as the summation of the length of the line segments of the total path. This is shown in Equation 6.2, where *n* is the number of segments the path was broken into for the calculation. In this case, it is equal to the number of simulation time steps.

$$Smoothness = \frac{\int_0^l (\frac{d\kappa}{dt})^2 ds}{t} \tag{6.1}$$

$$s = \sum_{i=0}^{n} \sqrt{(\Delta x_i)^2) + (\Delta y_i)^2 + (\Delta z_i)^2} \tag{6.2}$$

The curvature, κ, of a 3-dimensional point on a curve described by Cartesian coordinates is defined by Equation 6.3.

$$\kappa = \frac{\sqrt{(z''y' - y''z')^2 + (x''z' - z''x')^2 + (y''x' - x''y')^2}}{(x'^2 + y'^2 + z'^2)^{\frac{3}{2}}} \tag{6.3}$$

Hypothesis 2: Perceiving the closest gap in the environment for action will result in a shorter flight path.

The simulations described to test Hypothesis 1 are the same one hundred and twenty simulations used to test Hypothesis 2. During the 120 runs, an additional dependent variable of path length was also collected and analyzed. This metric is described in the subsection below.

6.1.2 Path Length

For mobile robot navigation, a trajectory is considered optimal when it is a straight line from the starting location to the goal location [72]. The path length utility metric described by Nowak [73] is used in the ethological literature [6] and in robotics literature [73], and [74] to compare the length of the flight path taken by the SUAS to the length

of a straight line from the starting location to the center of the gap traversed. This metric is calculated by taking the ratio of the distance traveled compared with the straight-line distance from the SUAS start location to the gap-center. This is the dependent variable, shown in Table 6.1, captured during the one hundred and twenty simulation runs and is reported as a percent difference of the average of the runs for each perceptual schema approach.

6.2 Results from Study 1

To test Hypothesis 1 the results of the three perceptual schema approaches are compared in terms of smoothness in Table 6.2. As introduced in Chapter 6, Hypothesis 1 is written below.

Hypothesis 1: Using a winner-take-all approach to perceive a gap in the environment for action will result in a smoother path.

Table 6.2: Results of the smoothness metric for three perceptual schema approaches over forty simulations to test Hypothesis 1

Perceptual Schema Approach	Smoothness
Winner-take-all: Closest	0.85
Winner-take-all: Largest	2.31
Summation: All	18.86

The table shows that the *detect_closest_gap* perceptual schema approach appears to be superior to the two others according to the smoothness metric. The *detect_closest_gap* perceptual schema approach completed forty simulation runs with the lowest average for the smoothness metric. The smoothness metric for the *detect_closest_gap* approach is the lowest at 0.85 with the *detect_largest_gap* measured at 2.31 and the *detect_all_gaps*

measured at 18.86. As seen in Table 6.3, both of the winner-take-all approaches are statistically better than the *detect_all_gaps* summation approach. The *detect_closest_gap* and *detect_all_gaps* t-test resulted in a value of 0.001 and the *detect_largest_gap* and *detect_all_gaps* t-test resulted in a value of 0.02. Between the two winner-take-all approaches the *detect_closest_gap* produces a statistically smoother path than the *detect_largest_gap* approach shown by the p-value of 0.008. These p-values prove the former perceptual schema approach is the best choice according to the smoothness metric.

Table 6.3: P-values computed from one-tailed two-sample t-tests for each combination of perceptual schema approaches

Perceptual Schema Approaches Compared	Smoothness p-values
Closest vs. Largest	0.008
Closest vs. All	0.001
Largest vs. All	0.02

The high value of the smoothness metric for the *detect_all_gaps* approach is likely due to having multiple instantiations of the *aim_gap_center* motor schema. The SUAS suffers oscillations in its flight path as one gap is not immediately preferred over all of the others. There is a potential the path could be smoothed by adjusting the gain used in the summation of the motor schema instantiations, but that was beyond the scope of these experiments.

Overall, the proof of statistical significance of the smoothness metric for the *detect_closest_gap* and *detect_largest_gap* winner-take-all approaches show we can accept Hypothesis 1. Meaning, the hypothesis is conclusive and using a winner-take-all approach to perceive a gap in the environment for action will result in a smoother path. The results obtained in simulation mirror the behavior seen in flying animals where a single gap is chosen

like the winner-take-all perceptual schema approaches implemented in this work. Additionally, these animals prefer to maintain a smooth and centered flight path providing further support to select one of the winner-take-all approaches of *detect_closest_gap*, or *detect_largest_gap* as the perceptual schema approach for implementation with the *gap_aiming* behavior as a proof-of-concept.

To test Hypothesis 2 the results of the three perceptual schema approaches are compared in terms of path length in Table 6.4. As introduced in Chapter 6, Hypothesis 2 is written below.

Hypothesis 2: Perceiving the closest gap in the environment for action will result in a shorter flight path.

The table shows that the *detect_closest_gap* perceptual schema approach appears to be superior to the two others. The *detect_closest_gap* perceptual schema approach completed forty simulation runs with the lowest average for the path length metric. The % difference between a straight line from the starting location of the gap center was only 9.18% greater compared with 12.68% for the *detect_largest_gap* and 13.73% for the *detect_all_gaps* perceptual schema approaches.

Table 6.4: Results of the two metrics for three perceptual schema approaches over forty simulations

Perceptual Schema Approach	Path Length
Winner-take-all: Closest	9.18%
Winner-take-all: Largest	12.68%
Summation: All	13.73%

Running a one-tailed, two-sample t-test for each combination of path length values with an α of .05 provides the p-values shown in Table 6.5. Because the path length metric

p-values for the t-tests completed between the *detect_closest_gap* and *detect_largest_gap*, and the *detect_closest_gap* and *detect_all_gaps* perceptual schema approaches are .01 with 99% confidence there is statistical significance between the measurements. The *detect_closest_gap* is the best approach according to path length. Intuitively, this makes sense where choosing the closest gap would lead to the shortest path. There is no statistical significance between the *detect_largest_gap* and *detect_all_gaps* approaches as shown by a p-value of 0.33 in Table 6.5.

Table 6.5: P-values computed from one-tailed two-sample t-tests for each combination of perceptual schema approaches

Perceptual Schema Approaches Compared	Path Length p-values
Closest vs. Largest	0.01
Closest vs. All	0.01
Largest vs. All	0.33

6.3 Proof-of-Concept: Hardware Implementation

The proof of concept implements the gap-aiming behavior described in Chapter 5 on a 3DRobotics Solo quadrotor, shown in Figure 6.1. This implementation uses the best perceptual schema approach determined through simulation in Study 1, *detect_closest_gap*. This hardware implementation demonstrates repeatable, autonomous, collision-free flight on the 3DRobotics Solo quadrotor in a restricted maneuverability environment using a visual sensor with no a priori knowledge, and completing all processing on-board. The purpose of this demonstration is stated formally, below.

Demonstration: Demonstrate the gap-aiming behavior produces repeatable autonomous flight on a small unmanned rotorcraft using on-board processing in an environment comparable to flying animal experiments and representative of an indoor disaster scenario.

Figure 6.1: Depiction of the 3DRobotics Solo quadrotor with GoPro Hero4 payload

The gap-aiming behavior designed from observations of flying animals and tested in simulation through Study 1 was used in this proof-of-concept implementation. The 3DRobotics Solo quadrotor platform and GoPro Hero4 Silver visual sensor payload were used. The field experiments were split into two sets. The first set consisted of ten runs with the same starting location to show repeatability and test the perceptual schema approach. The second set of field experiments consisted of five runs with an expanded experimental environment and varying starting location to show the motor schema produces three dimensional movement and determine the accuracy of the APF.

To provide the analysis three dependent variables were collected. These are the distance to the gaps for selection, the horizontal and vertical distance travelled, and the distance from the center of the gap during traversal. The distance to the gaps metric is measured using image coordinates on a frame taken from the live video feed of the GoPro. The change in x and y from the center of the image, which is the Solo's eye-view, and the center of the gap is used in the Pythagorean theorem to calculate the hypotenuse as shown in Figure 6.2 All of these hypotenuse calculations are compared and the smallest is selected as the closest gap.To facilitate understanding and comparison, the image coordinates are

translated and reported in centimeters.

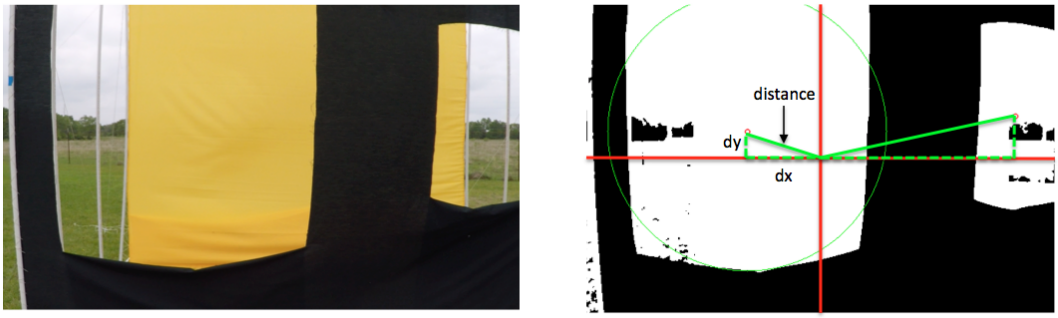

Figure 6.2: (a) Original image from the on-board GoPro video (b) Calculation of distance to each gap perceived in the FOV

The horizontal and vertical distance travelled is also calculated on a frame pulled from the video and calculated in image coordinates. The horizontal distance is equal to the change in x and the vertical distance is equal to the change in y shown in Figure 6.2. Again, this is translated and reported in centimeters to facilitate understanding and comparison. The distance from the gap center is also measured in image coordinates using third-person camera views of the flight. The location of the 3DRobotics Solo quadrotor in the image and the location of the gap center is identified and the difference is calculated. An example of the calculation of this metric for one of the field trials is shown in Figure 6.3. This metric is also translated into centimeters.

This proof-of-concept will maintain the constant value of five controlled variables: platform, visual sensor, the layout of the environment with respect to the scale, tortuosity, and the location f the gaps. These dependent and controlled variables are also summarized in Table 6.6.

Figure 6.3: (a) Image from third-person camera view of 3DRobotics Solo traversing the first panel (b) Image from third-person camera view of 3DRobotics Solo traversing the second panel

6.3.1 Proof-of-Concept Experimental Environment

While the *gap_aiming* behavior was designed from three suggestions for control of a SUAS recognized during the review of the ethological literature there was a major question left unanswered about the experimental environment. How are the environment and obstacles contained in the environment quantitatively defined?

Each of the fourteen articles discussing avoidance in the ethological literature made reference to clutter, but none defined what they considered a cluttered versus an uncluttered environment. The experimental environment navigated by the pigeons in [6] was called cluttered because it contained fifteen poles of 3.81 centimeter diameter in a 3 by 3 meter flight arena. While the papers reviewed on locusts and honeybees mentioned clutter, it was not described in specific terms, like the pigeon experiments. Robertson [36] likened a locust swarm to a complex environment requiring “effective and speedy motor control". The navigating abilities of the honeybee were tested in “an environment cluttered with obstacles” where the clutter is described as “an artificial meadow" [43].

As discussed in Section 2.4 during the review of the literature on reactive control for

Table 6.6: Description of variables to be varied, measured, and controlled in the proof-of-concept implementation

TYPE OF VARIABLE	VARIABLE	VALUE
Independent	Panels	One or Two
	Starting Location	Each of 4 quadrants Nominal flying zone: 1.17m
Dependent	Distance to Gaps	Reported in cm
	Horizontal Distance Travelled	Reported in cm
	Vertical Distance Travelled	Reported in cm
	Distance from Gap Center	Reported in cm
Controlled	Platform	3DRobotics Solo
	Sensor	GoPro Hero4 Silver
	Scale of Region	Restricted maneuverability
	Tortuosity	Actual Disaster Environment: 0.6
	Location of Gaps	Two gaps on each cloth wall sized for restricted maneuverability scale

obstacle avoidance in UAS none of the techniques were tested in indoor environments containing more than two obstacles, which were placed side-by-side. Additionally, no consistent metrics were used to define the experimental environments. The lack of description and non-existent quantitative metrics makes both the recreation of the testing scenarios and the direct comparison of the performance of the autonomous flight impossible.

To quantitatively define the environment, the design of the proof-of-concept environment will take into account the scale of the region and the traversability attribute of tortuosity to define the operational area available to the SUAS as described in [1]. The *scale of the region* is defined as the relationship between the size of the SUAS and the environment. The *traversability of the region* is not concerned with whether, or not, the SUAS is able to fit between obstacles, but if it can move through the environment. One measure of traversability will be used to design the environment: tortuosity. The *tortuosity* of the environment is a measure of the number of turns the SUAS is required to make over the

entire distance travelled.

6.3.2 Scale of a Region

In the ethological literature reviewed, pigeons and big brown bats were able to navigate collision-free in a region measured as *restricted maneuverability*. This was described in detail in Section 4.1 and is computed by Equation 6.4. The proof-of-concept environment is designed to create a restricted maneuverability scenario for a 3DRobotics Solo quadrotor and discussed in detail in Section 6.3.

$$2 * (\text{effective agent size}) > \text{environment} > \text{effective agent size} \tag{6.4}$$

6.3.3 Tortuosity of Environment

A greater tortuosity value means a greater number of turns are required over the distance travelled. To demonstrate the autonomous collision-free flight produced by the gap-aiming behavior would compare to flying animal experiments and be useful indoors in a disaster scenario a tortuosity representative of a disaster environment was used. This is described in detail in Section 6.3.

6.3.4 Quantitatively Defined Proof-of-Concept Environment

To demonstrate autonomous collision-free flight an environment quantified by the scale of region and tortuosity metrics was used in field tests with the 3DRobotics Solo. The first set of field experiments used one cloth panel. This environment contains two portions removed to simulate gaps and another solid panel as a backdrop to simplify the perception problem. This setup with the shape, location, and size of the gaps portrayed in Figure 6.4.

The second set of field tests used two cloth panels with shape, location, and size of the gaps and an additional solid panel as a backdrop to simplify the perception problem portrayed in Figure 6.5. The location of the gaps and varied starting locations produced

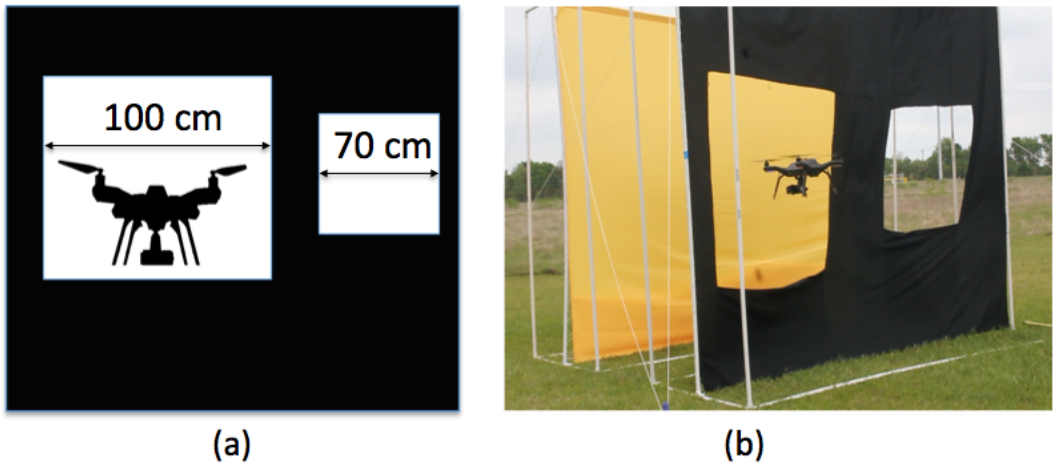

Figure 6.4: (a) Fabric panel with two gaps measured to create restricted maneuverability environment (b) Image of 3DRobotics Solo quadrotor traversing a gap during the first set of field trials

horizontal and vertical movement during flight tests. Cloth was chosen with the intent of reducing the possibility of causing damage to the hardware platform if a collision occurred.

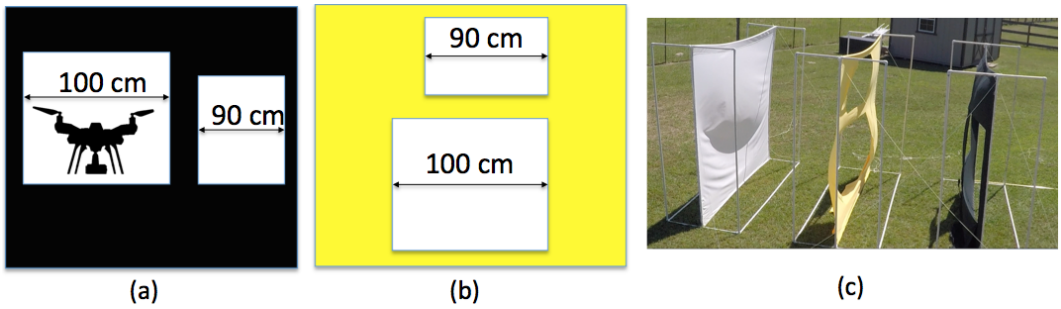

Figure 6.5: (a) First fabric panel with two gaps measured to create a restricted maneuverability environment (b) Second fabric panel with two gaps measured to create a restricted maneuverability environment (c) Overview image of flight environment for second set of field tests

To create the tortuosity of the environment during the field tests the panels were spaced 1.65 meters apart. This created the tortuosity measured from a review of literature con-

ducted on indoor disaster environments [3]. In Michael's work from the University of Pennsylvania, a ground robot and UAS robot team were used to survey a portion of the interior of a building at Tohoku University damaged after the 2011 earthquake in Japan [61]. Agarwal measured the tortuosity of this structure as 0.6.

As a reminder, the testing environments of current implementations had an average length of four meters when obstacles were present. While this experimental environment appears slightly shorter, it should be noted that in the related work there was only one, or two obstacles placed side-by-side. This created a tortuosity of 0.3 in the greatest case. The configuration of the obstacle(s) would be akin to having one panel with a gap like the first set of field tests. The amount of unoccupied space in the related works would be considered a habitable region where an SUAS could move freely, or was unknown. These two sets of field tests have a greater tortuosity within a restricted maneuverability environment.

6.4 Results of First Set of Field Tests

The field experiments are conducted using a 3DRobotics Solo quadrotor hardware platform shown in Figure 6.6a. This quadrotor is 56 cm from blade tip to blade tip, weighs 1.5 kg without a payload, has a payload capacity of 800 g, and a reported maximum speed of 89 km/hr [75]. It runs the APM autopilot software on a Pixhawk 2, carries a GoPro Hero4 Silver on a gimbal as the vision sensor, and runs an iMX6 companion computer with a Yocto Linux operating system. The GoPro weighs 84 g and measures 41 mm high by 59mm wide by 29.6 mm deep. The settings used for the GoPro are shown in Table 6.7.

The flight environment design is manufactured to simplify the perception problem, but uses the scale of the region attribute from disaster robotics [9] to quantify the operational area. Scale of the region describes the relationship between the effective size of the agent and the environment. The scale of the region where pigeons and big brown bats flew

Figure 6.6: (a) 3DRobotics Solo quadrotor platform used for flight experiments (b) Illustration of fabric panel with openings cut for gaps

Table 6.7: GoPro Hero4 Silver camera settings for proof-of-concept testing

Resolution	720p
Field of View	Narrow
Low Light	Off
White Balance	Auto
ISO	400
Protune	On

during experiments was measured as restricted maneuverability. This means the flight environment is greater than the size of the agent, but less than two times its size: *effective agent size* < Environment < *2 * effective agent size*. Because this work was inspired by flying animals, the scale of the region for the experimental environment was chosen to match that used in the flying animal experiments to demonstrate the gap-aiming behavior can produce autonomous, collision-free flight in a comparable environment. In terms of the 3DRobotics Solo quadrotor used for the demonstration, this equates to the smallest area in the flight environment being between 56 and 112 cm in width.

To create this flight environment, a black fabric panel 2.64 meters wide and 2.1 meters tall was used. Fabric was chosen to avoid damage to the platform if a collision should

occur. Openings were cut in the panel to create a restricted maneuverability environment where one opening is 70 cm wide and one is 100 cm wide. This is shown in Figure 6.6b These openings are the gaps perceived through blob detection using OpenCV onboard the 3DRobotics Solo.

The experimental flight begins with an autonomous takeoff 1.65 meters in front of the first panel containing the gaps. It autonomously takes off in the center of the panel to a height of 1.17 meters, which is the starting location for these 10 flights. This is the nominal flying height in an indoor office setting as measured by Agarwal [3]. An image of the starting location is shown in Figure 6.7a. From this location the the gap-aiming behavior outlined in Figure 6.8 is invoked to locate and traverse the gap. Figure 6.7b shows the 3DRobotics Solo quadrotor traversing the gap during a field trial. Once the platform has visually cleared the gap it is manually landed between the two panels.

Figure 6.7: (a) 3DRobotics Solo pictured at the starting location (b) 3DRobotics Solo shown traversing the gap

Using the gap-aiming behavior inspired by flying animals and described in this paper, the 3DRobotics Solo quadrotor successfully completed 10 autonomous flights in the ex-

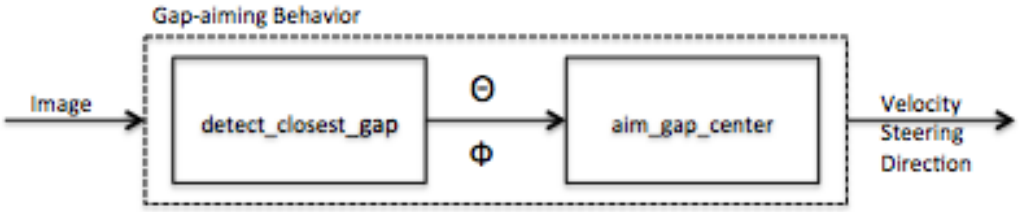

Figure 6.8: Flying animal inspired gap-aiming behavior with winner-take-all perceptual schema approach: *detect_closest_gap*

perimental environment. The intention of these experimental runs was to verify the coded implementation of the perceptual schema approach correctly selected the closest gap when the gap-aiming behavior was initially invoked. Additionally, these ten field experiments were used to show the performance of the gap-aiming behavior was repeatable. To show these, the experimental runs all began at the same starting location, which was centered width-wise on the panel at a distance of 1.65 meters from the panel, and an altitude of 1.17 meters. To be considered a successful flight, the platform must takeoff and traverse the gap with no human intervention and no collisions with the fabric panel. Due to autonomous takeoffs, there was variation in the starting location and the platform was not at the exact specified starting location each time. This is evidenced by the distance measurements shown in Table 6.8 when the perceptual schema initially selects the closest gap.

The values in Table 6.8 were plotted and are shown in Figure 7.1. Here, the triangle shaped points denote the left gap correctly selected initially as the closest perceived by the platform and the diamond-shaped point denotes the right gap was selected. From the robot's eye-view, the closest gap was initially selected for these ten flights showing the perceptual schema is performing as the implementation was intended.

Table 6.8: Results of the gap selection for the first set of field experiment flights.

FLIGHT	DISTANCE TO LEFT GAP	DISTANCE TO RIGHT GAP
1	60.53 cm	56.23 cm
2	45.15 cm	64.13 cm
3	36.21cm	61.94 cm
4	49.77 cm	61.61 cm
5	39.74 cm	75.07 cm
6	49.03 cm	59.67 cm
7	48.05 cm	64.93 cm
8	55.18 cm	65.70 cm
9	43.11 cm	67.54 cm
10	47.57 cm	61.83 cm

6.5 Results of Second Set of Field Tests

The second set of field tests were conducted with the same platform and sensor setup discussed in Section 6.4. This set consisted of five flights in a restricted-maneuverability environment containing two fabric panels with gaps. These gaps create a restricted maneuverability environment where the largest gap is 100 cm x 100 cm. The width of the Solo from blade to blade is 56 cm, which computes to a characteristic dimension of 1.79. Simply stated, the gap is 1.79 times larger than the platform. The 90 cm gap has a characteristic dimension of 1.61. It is described in detail in Section 6.3.4. This set of field tests utilized five different starting locations as shown in Figure 6.9. The purpose of the differing starting locations was to show the three dimensional movement produced by the motor schema.

6.5.1 Motor Schema Evaluation

The horizontal and vertical distance travelled during a flight were calculated to demonstrate the three dimensional movement of the motor schema, implemented with an APF described in Section 5.2.2. The total distance travelled is an approximation of the distance

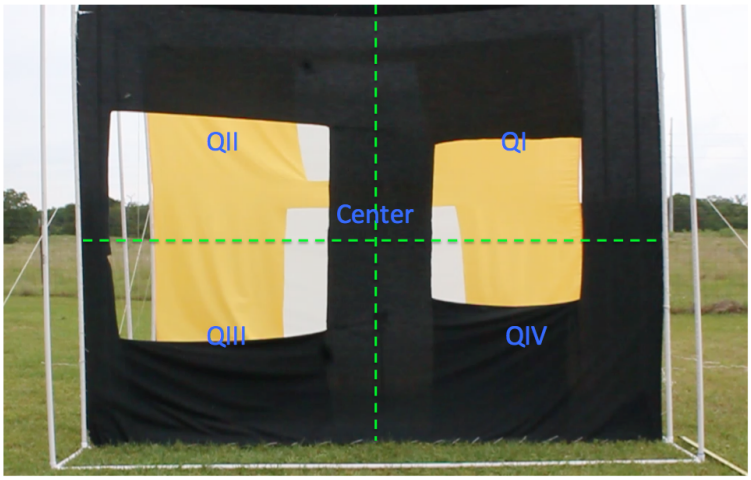

Figure 6.9: Starting locations for the second set of field tests. The center represents the nominal height of 1.17 meters measured by [3] in an indoor office scenario.

Table 6.9: Distance travelled horizontally and vertically during a flight through both panels in the second set of field trials.

STARTING QUADRANT	PANEL 1 DIST TRAVELLED HORZ / VERT	PANEL 2 DIST TRAVELLED HORZ / VERT	TOTAL TRAVELLED HORZ / VERT
Center	42.69 cm / 8.54 cm	57.98 cm / 6.44 cm	100.67 cm / 14.98 cm
I	29.8 cm / 29.73 cm	62.96 cm / 26.97 cm	92.76 cm / 56.7 cm
II	13.27 cm / 55.86 cm	60.89 cm / 17.64 cm	74.16 cm / 73.5 cm
III	19.33 cm / 40.35 cm	54.75 cm / 8.02 cm	74.08 cm / 48.37 cm
IV	28.21 cm / 31.21 cm	53,57 cm / 28.42 cm	81.78 cm / 59.63 cm
		AVERAGE:	**84.69 cm / 50.64 cm**

from the starting location to the point where the platform traverses the gap in the second panel. It is calculated from images taken from the on-board video. The values for horizontal and vertical movement to the traversal point in each panel are shown in Table 6.9. Additionally, the total distance and averages are also reported.

Overall, the panels are 264 cm wide by 210 cm tall and the largest average distance travelled during this set of field trials was 100.67 cm horizontally from a center starting

Figure 6.10: Time-lapse image created from overview video taken during a flight starting in quadrant IV.

location and 73.5 cm vertically from a starting location in Quadrant III. This three dimensional movement is shown in Figure 6.10, which provides a view of the 3DRobotics Solo quadrotor in a still image at different points during a flight. This image was created from an overview video taken during the flight starting in quadrant IV. The total horizontal movement during this flight was 81.78 cm and the total vertical movement was 59.63 cm as reported in Table 6.9. The calculation of the horizontal and vertical distance travelled for each of the five flights with different starting locations confirms the gap-aiming behavior produces movement in three dimensions.

The intention of the novel APF implementation is to provide a smooth trajectory and the largest safety margin available for clearance by traversing at the center of the gap. To show the APF is both performing as expected by centering the platform for gap traversal and is a useful implementation of the gap-aiming seen in flying animals, the accuracy of the alignment with the center of the gap through actions produced by the APF is determined.

Table 6.10: Distance from the center of the gap both horizontally and vertically for each panel over five flights.

STARTING QUADRANT	PANEL 1 DISTANCE FROM GAP CENTER HORIZONTAL / VERTICAL	PANEL 2 DISTANCE FROM GAP CENTER HORIZONTAL / VERTICAL
Center	8.91 cm / -14.95 cm	-13.31 cm / 22.64 cm
I	13.46 cm / 7.12 cm	11.79 cm / -6.19 cm
II	-16.81 cm / 1.2 cm	-0.89 cm / 12.65 cm
III	2.43 cm / -6.72 cm	9.15 cm / -14.62 cm
IV	9.61 cm / 4.05 cm	16.45 cm / -4.94 cm
MEAN ERROR:	**3.52 cm / -1.86 cm**	**4.64 cm / 1.91 cm**

This is done by calculating the distance from the center of the selected gap was calculated in images taken from third-person camera views as the platform traversed the gap in each panel. To determine when the platform was traversing the gap, the on-board video and third-person camera view were aligned. When the platform no longer had the panel in view from the on-board video a frame was taken from the third-person view video to calculate the distance from the center of the gap. At this point in the flight, because the panel is no longer in view, the motor schema would not command any horizontal, or vertical movements to continue aligning the platform. These calculations for the second set of field tests are reported in Table 6.10.

6.6 Summary

This chapter discussed the Study 1 completed via simulation to determine the best perceptual schema approach to use for the proof-of-concept demonstration. Two hypotheses were tested and evaluated using the smoothness and path length metrics to statistically show the best approach for use in the demonstration is detect_closest_gap. This was followed with a discussion of the variables for the proof-of-concept demonstration, with three calculated metrics used to evaluate the field experiments. The experimental environment

was described in Section 6.3.1 and the results presented in Section 6.5. The next chapter provides a discussion and analysis of those results.

7. DISCUSSION

This chapter discusses and interprets the results of the field experiments evaluated through the use of three calculated metrics previously presented in Chapter 6. The results of the field experiments showed the gap-aiming behavior successfully produced repeatable, autonomous flight on small unmanned quadrotor in a restricted maneuverability environment using a novel artificial potential field. The next section discusses the robustness of the reactive behavior through gap selection with insights for ethology following in Section 7.1.1. Section 7.2 analyzes the measurements calculated for the gap traversal. Section 7.3 compares the field experiment results with the simulation completed in Study 1. The impact of modifying the implementation of the gap-aiming behavior is discussed in Section 7.4 and the novelty of the APF implemented in this work is discussed in Section 7.5. Section 7.6 provides ideas for the low-level control of a platform for future work. Finally, the chapter concludes with a summary in Section 7.8.

7.1 Gap Selection

Because the starting location of the ten flights conducted in the first set of experiments was inexact, the entirety of both gaps was not in the robot's eye view. Therefore, what the platform perceived as the center of the gap was not the true center of the gap. Table 7.1 shows the true distance of the gaps from the platform during this initial calculation. The points are again plotted on a graph shown in Figure 7.2. In the case of these ten flights, the ground truth closest gap still matches with what was perceived as the closest gap by the platform during the experimental flight.

When the initial calculation was made to determine the closest gap in the field of view, one outlier is shown on both graphs in Figures 7.1 and 7.2. This is the first flight where the right gap is initially selected. Because it was an outlier, this particular flight was

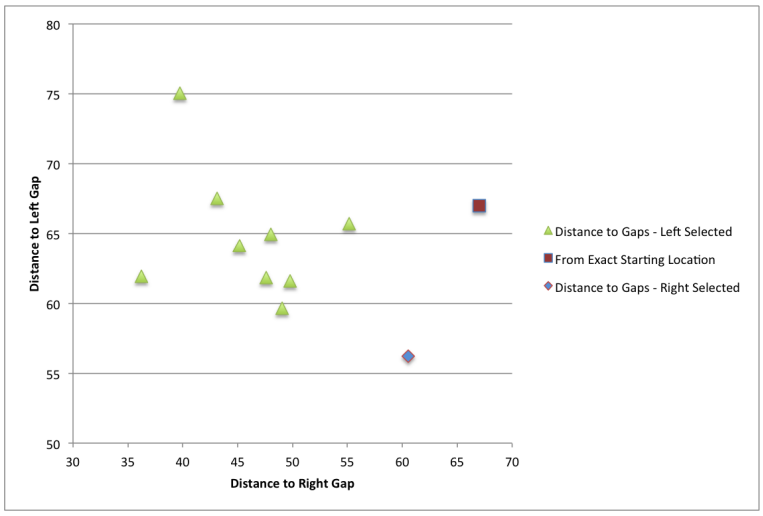

Figure 7.1: This graph shows the distance from the platform to the perceivable gaps when the gap-aiming behavior is initially invoked.

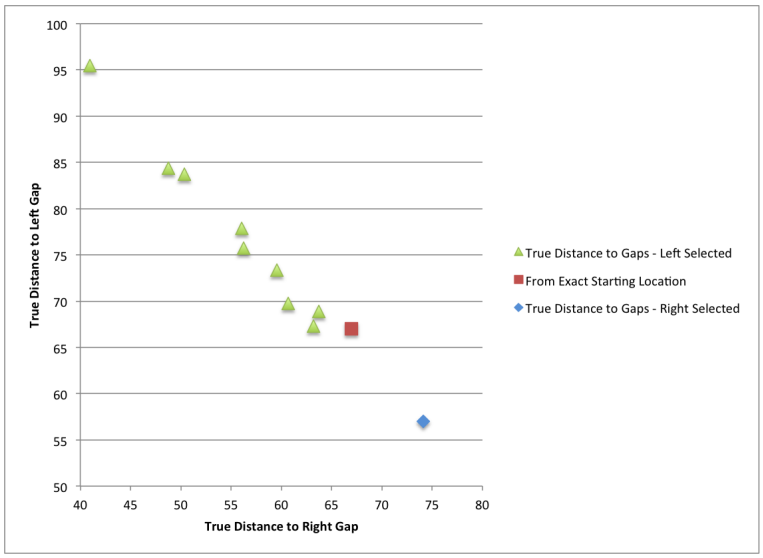

Figure 7.2: This graph shows the true distance from the platform to the perceivable gaps when the gap-aiming behavior is initially invoked.

further investigated. After reviewing the video and the weather notes taken for that day, it became apparent that immediately following this right gap selection a gust of wind pushed

Table 7.1: Results of the first set field experimental flights.

FLIGHT	TRUE DISTANCE TO LEFT GAP	TRUE DISTANCE TO RIGHT GAP
1	74.11 cm	56.99 cm
2	56.07 cm	77.87 cm
3	48.75cm	84.38 cm
4	60.70 cm	69.77 cm
5	40.96 cm	95.45 cm
6	63.71 cm	68.91 cm
7	56.26 cm	75.73 cm
8	63.22 cm	67.28 cm
9	50.39 cm	83.71 cm
10	59.57 cm	73.33 cm

the platform to the left. The wind was a constant 10 mph out of the SSE with 24 mph gusts. As the gap-aiming behavior continually re-evaluated the flight environment the left gap became the closest and the motor schema commanded the platform towards this gap center. This flight ended in the left gap being traversed and it is a good representation of the robustness of the reactive behavior.

7.1.1 Insights for Ethology

The wind experienced during the field trials, which caused the swap in the gap selected for traversal during the flight discussed above, is one possible explanation for the lack of clarity on a perceptual schema approach in the ethological literature. In the observations of flying animals it may not have been possible to determine when the animal was reacting to a particular gap due to its size, closeness, or other reason and when the wether was the deciding factor. It could be concluded that the detect_all_gaps approach may be the best approach with the gains tuned to direct a winner-take-all outcome like the other approaches.

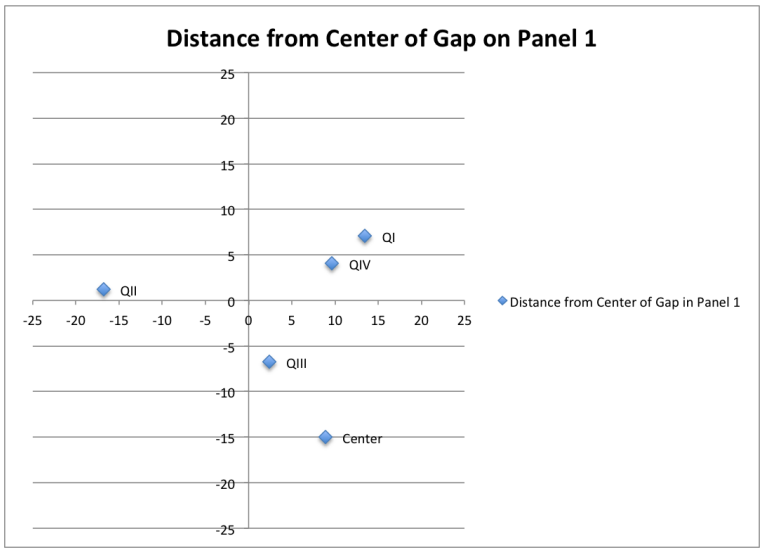

Figure 7.3: The graphs plots the location where the platform traversed the second panel by showing distance from the center of the gap.

7.2 Gap Traversal

The metric computed to determine the distance from the center of the gap during traversal and reported in Table 6.10 resulted in mean error values close to, but not at zero in all cases. To help visualize whether there was any bias in the alignment produced by the artificial potential field two graphs are provided in Figures 7.3 and 7.4. The first reports measurements for the first panel and the second reports the measurements for the second panel. They use the same scale, where the center of the gap is at the origin and the axes extend 25 cm in each direction. The five flights are plotted at the location where their gap traversal was measured.

While the sample size is really too small to statistically claim there is no bias, this data leads us in that direction because if bias existed you would expect to see the flights clustered in the same location on the graph, which is not the case. However, further investigating was conducted to determine if there was a reason to attribute to the slightly uncentered

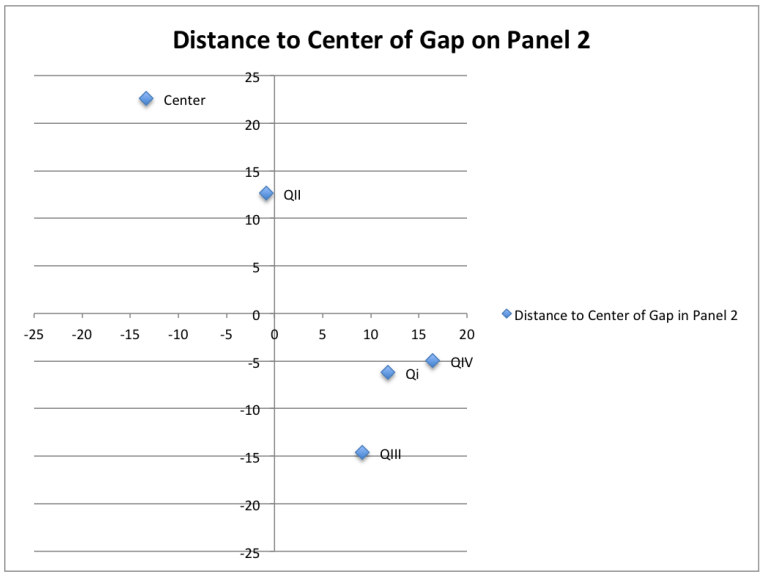

Figure 7.4: The graphs plots the location where the platform traversed the second panel by showing distance from the center of the gap.

traversals. Because the calculations presented initially suggest the APF was not accurately aligning the platform for flight through the gap, the on-board video was used to recreate the APF output during the flight and compared with a review of the matching overview video to determine the underlying cause. Figure 7.5a shows the perceptual schema identifying the closest gap and the resultant vector output from the APF, which commands the platform to move left, right, and forward. Figure 7.5b is the next frame pulled from the video where the platform was pushed by a gust of wind. As shown, the platform was pushed in a direction conflicting with what the gap-aiming behavior commanded. The day the flight shown in Figure 7.5 was conducted the wind maintained a constant 1.2 mph out of the south with 6.2 mph gusts, also out of the south. Because these field trials were conducted outside the wind gusts had an affect on the movement of the platform, which leads to a reasonable assumption about wind causing non-centered gap traversals as shown in Table 6.10.

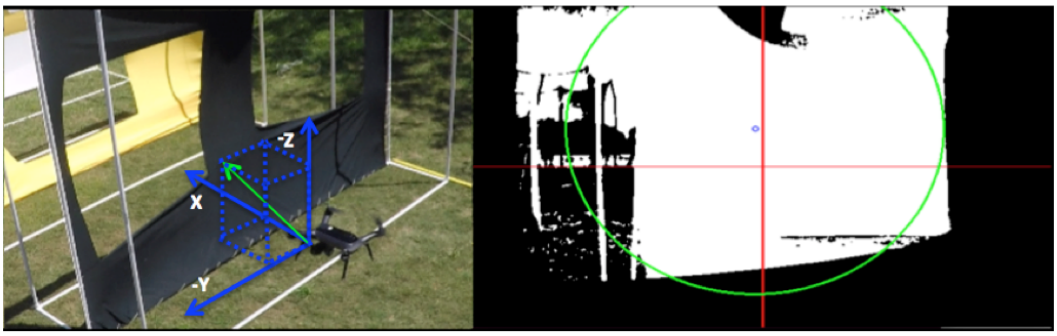

(a)

(b)

Figure 7.5: (a) Overview video shown side-by-side with onboard video. Perceptual schema identified the closest gap and the resultant vector from the APF is shown on the left. (b) Overview video and side-by-side on-board video showing the wind affected the movement of the platform in a direction different from the APF command.

This work assumed that all gaps in the 3DRobotics Solo quadrotor FOV were large enough for the platform to traverse. In the future, an accurate measurement of the distance a platform is uncentered during traversal, potentially measured with a motion-capture system, could be used to inform a buffer distance required when selecting which gaps are large enough for the platform to traverse. Additionally, this ground-truth information could be used to tune the magnitude profiles of the artificial potential field to prefer alignment with the gap center over attraction to it.

7.3 Simulation vs. Field Experiments

In hindsight, the results of the simulation used to determine the best perceptual schema approach to implement with a gap-aiming behavior for the proof-of-concept demonstration might not be directly applicable to the field experiments because no environmental factors were simulated. During the field experiments, the wind was shown to be a factor affecting the gap selection and centering for gap traversal. However, if we consider the possibility the wind consistently affected the platform across all flights, then the analysis of the simulation flights resulting in detecting the closest gap producing the statistically shortest and smoothest path would hold. To create a simulation to test the effects of the wind on the perceptual schema approaches the platform and its dynamics would need to be correctly modeled as well as the wind. Overall, the complication of ensuring and proving the environmental factors and platform were correct in the simulation would be less beneficial than testing other perceptual schema approaches directly on the platform. This leads to the conclusion that investigating ways to improve the field experiments would be a better use of time and resources.

The smoothness and path length metrics were selected to evaluate the Matlab®simulation because of the interest in the SUAS community to reduce energy expenditure and produce time savings with both a smooth and a short flight path. Using the same metrics would

have informed the field experiments, but no motion capture system was available to provide ground truth for their calculation. This is discussed in Section 8.1 and left for future work. What could improve the simulation is if speed was considered a factor for gap selection. The perceptual schema approach shown to be superior when speed was factored in would provide a useful counterpart to the field experiments.

7.4 Impact of Gap-Aiming Behavior Modifications

This section speculates on the impacts of implementing a different perceptual schema, or maintaining local map of the environment. First, a more sophisticated perceptual schema is required to test the gap-aiming behavior in another flight environment not designed with perceptual simplicity in mind for the field experiments conducted in this work. It is reasonable to assume a more computationally efficient algorithm, or more processing power on the platform would enable operation at greater frames per second and therefore, produce higher platform speeds safely. A local map of the world, which could keep a predetermined number of seconds of sensor readings could potentially allow the platform to recover from a local minima. This may be possible by introducing a behavior for backtracking when no gaps are perceivable.

7.5 Novel Artificial Potential Field Implementation

Compared with other APF implementations on SUAS for autonomous collision-free flight, this research implements a novel artificial potential field to produce movement in three dimensions with no buffer distance required in a restricted maneuverability environment. It uses both a selective attractive and tangential field to aim the SUAS to the center of a gap in the FOV of the visual sensor used. In this way, the APF implicitly avoids obstacles in the environment without the use of a repulsive field common to all other implementations. This gap-aiming behavior is inspired by the same behavior observed in flying animals and reported in the ethological literature.

In contrast to the novel APF implementation in this research, current implementations of artificial potential fields for autonomous flight on SUAS operate in only two dimensions, require a buffer distance incompatible with a restricted maneuverability environment, or use the traditional APF with a repulsive field for obstacles. Additionally, none of the current implementations make use of a tangential field, or are tested in a restricted-maneuverability environment. For example, Woods implemented a controller he termed an extended potential field, which tracks a target while avoiding obstacles in the flight path [76]. Avoidance maneuvers are conducted in only two dimensions and a 0.5 meter buffer distance is maintained between the platform and the obstacle. Using a fixed-wing, Ruiter avoided obstacles by bounding them with enlarged rectangles and either selecting a path to fly over or around them, but never making a three dimensional maneuver [77]. Additionally, while the platform could increase its altitude to fly over an obstacle, it would never decrease altitude to fly under because the rectangles bounding the obstacles were always enlarged all the way to the ground. A traditional APF using an attractive field for the goal and repulsive field for obstacles was implemented by Nieuwenhuisen [12]. There was no direct discussion of three dimensional versus two dimensional movement; however, the obstacle avoidance experiment used to demonstrate the APF implementation was a platform hovering and not colliding with a yellow sheet moved towards it. This leads to the impression the platform was experiencing a repulsive force from the sheet and moving opposite until reaching an unreported buffer distance. Another traditional APF was also implemented by Grzonka [15]. A safety margin is mentioned in the report, but not enumerated. Additionally, when an avoidance maneuver is shown in images the movement of the platform is around the object with the flight path being adjusted in only two dimensions.

While the implementation in this research is simpler with no repulsive field, and shown to produce movement in three dimensions while operating in a restricted maneuverability environment suggesting it is superior to current implementations the performance com-

parison between implementations using quantitative metrics was outside the scope of this research. In the future, with the use of a motion capture system the flight trajectory could be accurately tracked to compute path length, smoothness, gap (obstacle) clearance, and flight time. These measurements could be used to compare the performance with other implementations although ensuring a fair comparison may mean recreating the other implementations on the same platform and testing them in the same environment to reduce the number of variables affecting the performance.

7.6 Control Aspects

The benefit of a smooth flight path created through the use of an APF for a quadrotor platform with the ability to stop and change directions may seem unnecessary, but smoothness is still a consideration because it could result in both reduced energy expenditure and time savings. The motor schema of the gap-aiming behavior described in this work is implemented with an artificial potential field, but it is not specifically evaluated for smoothness because ground-truth measurements were not available. However, the novel APF implementation used in this work lacks a repulsive field employed for obstacles in the environment like standard implementations, which could remove the significant problem of "oscillations in the presence of obstacles" observed by Koren and Borenstein [78].

While low-level control of the quadrotor was beyond the scope of this research, the APF implementation does provide high-level velocity control. Calculated on the onboard iMX6 companion computer, the output of the APF is a vector with magnitude and direction for control of the 3DRobotics Solo quadrotor in the field experiments. The low-level attitude control providing commands to the ESCs to produce pitch, roll, and yaw is handled by the ArduCopter flight stack, which uses a PID controller running on a PixHawk and is tuned for the 3DRobotics Solo.

With knowledge of the dynamics of the platform, the magnitude profiles that used

angle measurements corresponding to the FOV of the onboard visual sensor could be fine-tuned to ensure no magnitude would be commanded that could destabilize the platform, or attempt to produce a trajectory outside of the ability of the platform. Additionally, taking into account the dynamics of the platform, a gain could be developed for the attractive and tangential field with the ability for each field to affect the gain of the other, or maintain a ratio between the two, when the computed vector commands an unobtainable trajectory. The implementation of this gap-aiming behavior was not specifically tuned for the platform used in the field experiments. Because of this, it is extensible to any platform, but will a require a more sophisticated perceptual schema to produce the same autonomous flight in a less perceptually simplistic testing environment.

7.7 Improvements to Field Experiments

Fifteen flights were successfully completed in two sets of field experiments; however, making minor changes to the environment could have reduced the unintended environmental variables, and improved the collection of metrics. First, conducting the field experiments indoors would remove the wind effects and allow for analysis of the APF implementation without this variable. Enlarging the panels both horizontally and vertically would provide room for more gaps in each panel and potentially greater three dimensional movement of the platform. Additionally, the use of a motion capture system during the experiments would inform the calculation of quantitative metrics to analyze the performance of this gap-aiming behavior implementation.

7.8 Summary

The results of the 120 simulation runs conducted during Study 1 and the fifteen experimental flights of the gap-aiming behavior implementation on a 3DRobotics Solo quadrotor tested in a restricted maneuverability environment in the field were analyzed and discussed in this chapter. The statistical analysis of the simulation runs with two metrics showed the

detect_closest_gap was the best perceptual schema approach. This perceptual schema approach was implemented for the gap-aiming behavior on the 3DRobotics Solo. The first set of field experiments with the 3DRobotics Solo was ten flights through one panel with gaps creating a restricted maneuverability environment. These ten flights showed both repeatability and the robustness of the reactive behavior through gap selection. The second set of field experiments was five flights through two panels with gaps creating a restricted maneuverability environment. The ability of the novel APF to center the platform for gap traversal during these flights was analyzed. Taking into account the small sample size the data suggest the APF is unbiased and the environmental wind factor provides an explanation for the platform not being directly centered. Additional discussion is provided on insights for ethology, comparison of field experiment results with the simulation completed in Study 1, the impact of modifying the implementation of the gap-aiming behavior, the novelty of the APF implemented in this work, control aspects, and improvements that could be made to the field test environment.

8. SUMMARY AND FUTURE WORK

Collision-free autonomous flight is essential for the operation of a small unmanned aerial system in an indoor environment with restricted maneuverability typical of the interior of an office building after a natural, or man-made disaster. The addition of autonomy to the system enables flight beyond the line of sight of an operator, provides repeatable performance, and removes the human factor that could lead to mishaps whether during training, or mission operation [5].

Through designed experiments and observations in their natural habitat, biologists and ethologists reported on the ability of birds, bats, and insects to successfully navigate collision-free through environments with closely space obstacles [6, 7, 32, 44, 43]. Unlike current implementations on SUAS, flying animals produce reactive, collision-free flight by aiming towards open spaces, or gaps in their environment. This provides an existence proof that autonomous flight can be done collision-free at high speeds in restricted maneuverability environments.

This work described the implementation and testing of a *gap_aiming* behavior in simulation, concentrating on determining which of three possible perceptual schemas are best suited for controllable, efficient flight by testing Hypothesis 1 and 2 of the primary research question. One hundred and twenty simulation runs were completed with smoothness and path length metrics captured to compare the three perceptual schema approaches. The results are shown and discussed in Chapter 7. Overall, the *detect_closest_gap* and *detect_largest_gap* winner-take-all approaches produced statistical smoother paths than detecting all of the gaps in the FOV. The t-tests conducted with the values computed through the path length metric show the *detect_closest_gap* was statistically the best perceptual schema approach. This perceptual schema approach was chosen for the gap-aiming be-

havior implementation with an APF. Autonomous, collision-free flight was demonstrated in two sets of field tests in a restricted maneuverability environment.

These fifteen flights were evaluated with three calculated metrics: distance to the perceived gaps, horizontal and vertical movement, and distance from the center of the gap during traversal. Analysis of this data showed the perceptual schema correctly selected the closest gap 100% of the time, the motor schema produced three dimensional movement, and while the measurement form the center of the gap suggested the APF was inaccurate, an explanation with supporting data was provided.

Overall, the successful implementation and field testing of the *gap_aiming* behavior for reactive control of autonomous collision-free flight on a small unmanned quadrotor in restricted maneuverability environments contributes to the fields of artificial intelligence, robotics, and ethology as described in the introductory chapter. The description of the experimental testing environment quantified with metrics from disaster robotics, which reflects both the expected condition of the interior of a structure after a disaster and the flight environment of animals provides a benchmark for testing autonomous flight of SUASs.

8.1 Future Work

To further test and potentially improve the perceptual schema portion of the gap-aiming behavior there are four avenues to explore. First, if the goal location is known it could be taken into consideration when determining the gap for traversal. For instance, the closest gap could be considered the gap bringing the platform in line with the goal location rather than the gap closest to the current flight path. Second, gaps requiring a horizontal movement rather than vertical (or vice versa) could be preferred over the other. Third, speed could be taken into account during gap selection. When flying at higher speeds a larger gap might be preferred to ensure the safety of the platform. Finally, the perceptual schema could take into account hierarchical conditions when two, or more, gaps are determined to

be equally close to the platform. Regardless of whether any of these avenues are explored, a more sophisticated perceptual schema than the blob detection used in the field experiments should be implemented to allow the novel artificial potential field implementation to be tested in an environment not designed for perceptual simplicity.

To improve the performance of the artificial potential field two avenues could be explored in future work. First, in the current implementation the attractive and tangential fields are evenly applied. In the future, alignment with the center of the gap could be preferred over the attraction with the tangential field by introducing a gain applied to the magnitude calculation. Second, the magnitude profiles for both the selective attractive and tangential fields could be tuned either with knowledge of the dynamics of the platform, or empirically during field experiments.

In terms of platform improvement, a smaller and more agile quadrotor could be tested with the current implementation to see if it provided similar performance. To successfully compare the performance of the two (or more) platforms a motion capture system, or other means of providing ground truth, could be used. This would allow calculation of metrics like cross track error to determine how accurately the platform followed the expected path from a starting location to gap center.

REFERENCES

[1] R. R. Murphy, *An Introduction to AI Robotics*. A Bradford Book, 2000.

[2] http://ww.cs.cmu.edu/motionplanning/lecture/Chap4-Potential-Field_howie, 2007.

[3] S. Agarwal, R. Murphy, and J. Adams, "Characteristics of indoor disaster environments for small uass," in *Safety, Security, and Rescue Robotics (SSRR), 2014 IEEE International Symposium on*, pp. 1–6, Oct 2014.

[4] http://tech.co/drones-dull-dirty-dangerous-2014-11, 2014.

[5] A. P. Tvaryanas, W. T. Thompson, and S. H. Constable, "The u.s. military unmanned aerial vehicle (uav) experience: Evidence-based human systems integration lessons learned."

[6] H.-T. Lin, I. G. Ros, and A. A. Biewener, "Through the eyes of a bird: modelling visually guided obstacle flight," vol. 11, 2014. Journal of The Royal Society Interface.

[7] I. Cuthill and T. Guilford, "Perceived risk and obstacle avoidance in flying birds," *Animal Behaviour*, vol. 40, no. 1, pp. 188–190, 1990.

[8] R. Kern, N. Boeddeker, L. Dittmar, and M. Egelhaaf, "Blowfly flight characteristics are shaped by environmental features and controlled by optic flow information," *The Journal of Experimental Biology*, vol. 215, no. 14, pp. 2501–2514, 2012.

[9] R. R. Murphy, *Disaster Robotics*. The MIT Press, 2014.

[10] R. C. Arkin, *Behavior-Based Robotics*. The MIT Press, 1999.

[11] M. J. Matarić, *The robotics primer*. Intelligent robotics and autonomous agents series, Cambridge, Mass. : The MIT Press, 2007.

[12] M. Nieuwenhuisen, D. Droeschel, J. Schneider, D. Holz, T. Labe, and S. Behnke, "Multimodal obstacle detection and collision avoidance for micro aerial vehicles," in *Mobile Robots (ECMR), 2013 European Conference on*, pp. 7–12, Sept 2013.

[13] C. Yuan, F. Recktenwald, and H. Mallot, "Visual steering of uav in unknown environments," in *IEEE/RSJ International Conference on Intelligent Robots and Systems*, pp. 3906–3911, Oct 2009.

[14] T. Merz and F. Kendoul, "Dependable low-altitude obstacle avoidance for robotic helicopters operating in rural areas.," *Journal of Field Robotics*, vol. 30, no. 3, pp. 439–471, 2013.

[15] S. Grzonka, G. Grisetti, and W. Burgard, "A fully autonomous indoor quadrotor.," *IEEE Transactions on Robotics*, vol. 28, no. 1, pp. 90–100, 2012.

[16] S. Ross, N. Melik-Barkhudarov, K. Shaurya Shankar, A. Wendel, D. Dey, J. A. Bagnell, and M. Hebert, "Learning monocular reactive uav control in cluttered natural environments," in *IEEE International Conference on Robotics and Automation (ICRA)*, The Robotics Institute Carnegie Mellon University, 2013.

[17] C. Bills, J. Chen, and A. Saxena, "Autonomous mav flight in indoor environments using single image perspective cues.," in *Proceedings - IEEE International Conference on Robotics and Automation*, pp. 5776–5783, 2011.

[18] J.-C. Zufferey and D. Floreano, "Fly-inspired visual steering of an ultralight indoor aircraft.," *IEEE Transactions on Robotics*, vol. 22, no. 1, pp. 137 – 146, 2006.

[19] S. Hrabar, G. Sukhatme, P. Corke, K. Usher, and J. Roberts, "Combined optic-flow and stereo-based navigation of urban canyons for a uav.," in *IEEE/RSJ International Conference on Intelligent Robots and Systems*, vol. 1, pp. 302 – 309, 2005.

[20] A. J. Barry and R. Tedrake, "Pushbroom stereo for high-speed navigation in cluttered environments.," 2014.

[21] S. Scherer, S. Singh, L. Chamberlain, and M. Elgersma, "Flying fast and low among obstacles: Methodology and experiments.," *International Journal of Robotics Research*, vol. 27, no. 5, pp. 549 – 574, 2008.

[22] S. R. Kukreti and A. Sathyan, "Obstacle avoidance and location determination of an unmanned aerial vehicle in a gps-denied, hazard-cluttered indoor environment.," *International Journal of Unmanned Systems Engineering*, vol. 3, no. 2, pp. 75 – 99, 2015.

[23] S. Winkvist, E. Rushforth, and K. Young, "Towards an autonomous indoor aerial inspection vehicle.," *Industrial Robot*, vol. 40, no. 3, pp. 196–207, 2013.

[24] F. Wang, J.-Q. Cui, B.-M. Chen, and T. H. Lee, "A comprehensive uav indoor navigation system based on vision optical flow and laser fastslam.," *Acta Automatica Sinica*, vol. 39, pp. 1889 – 1899, 2013.

[25] D. Lee, M. Di Cicco, G. Grisetti, and D. Lee, "Dynamic window indoor navigation for a quadrotor using rgbd sensor," in *IEEE/RSJ International Conference on Intelligent Robots and Systems*, 2016.

[26] H. Alvarez, L. M. Paz, J. Sturm, and D. Cremers, *Collision Avoidance for Quadrotors with a Monocular Camera*, pp. 195–209. Cham: Springer International Publishing, 2016.

[27] N. Gageik, P. Benz, and S. Montenegro, "Obstacle detection and collision avoidance for a uav with complementary low-cost sensors," *Access, IEEE*, vol. 3, pp. 599–609, 2015.

[28] M. V. Srinivasan, "Strategies for visual navigation, target detection and camouflage: inspirations from insect vision," in *Proceedings., IEEE International Conference on Neural Networks*, vol. 5, pp. 2456–2460 vol.5, 1995.

[29] P. Arena, L. Fortuna, M. Frasca, and G. Sicurella, "An adaptive, self-organizing dynamical system for hierarchical control of bio-inspired locomotion," *IEEE Transactions on Cybernetics*, vol. 34, pp. 1823–1837, August 2004.

[30] J. Yu, M. Tan, S. Wang, and E. Chen, "Development of a biomimetic robotic fish and its control algorithm," *IEEE Transactions on Cybernetics*, vol. 34, pp. 1798–1810, August 2004.

[31] B. Fu, Y. Xiao, X. Liang, and C. P. Chen, "Bio-inspired group modeling and analysis for intruder detection in mobile sensor/robotic networks," *IEEE Transactions on Cybernetics*, vol. 45, pp. 103–115, January 2015.

[32] S. Sändig, H.-U. Schnitzler, and A. Denzinger, "Echolocation behaviour of the big brown bat (eptesicus fuscus) in an obstacle avoidance task of increasing difficulty," *The Journal of Experimental Biology*, vol. 217, no. 16, pp. 2876–2884, 2014.

[33] S. Shen, Y. Mulgaonkar, N. Michael, and V. Kumar, "Multi-sensor fusion for robust autonomous flight in indoor and outdoor environments with a rotorcraft mav," in *IEEE International Conference on Robotics and Automation (ICRA)*, GRASP Laboratory, University of Pennsylvania, 2014.

[34] J. Eklof, *Vision in Echolocating Bats*. PhD thesis, Goteborg University, 2003.

[35] M. V. Srinivasan, S. W. Zhang, J. Berry, K. Cheng, and H. Zhu, "Honeybee navigation: linear perception of short distances travelled," *Journal of Comparative Physiology A*, vol. 185, no. 3, pp. 239–245, 1999.

[36] R. M. Robertson and A. G. Johnson, "Collision avoidance of flying locusts: Steering torques and behaviour," *Journal of Experimental Biology*, vol. 183, no. 1, pp. 35–60, 1993.

[37] D. Eckmeier, B. R. H. Geurten, D. Kress, M. Mertes, R. Kern, M. Egelhaaf, and H.-J. Bischof, "Gaze strategy in the free flying zebra finch (taeniopygia guttata)," *PLoS One*, vol. 3, no. 12, 2008.

[38] P. Bhagavatula, M. Ibbotson, M. Srinivasan, and C. Claudianos, "Optic flow cues guide flight in birds.," *Current Biology*, vol. 21, no. 21, pp. 1794–1799, 2011.

[39] D. N. Orbach and B. Fenton, "Vision impairs the abilities of bats to avoid colliding with stationary obstacles," *PLoS ONE*, vol. 5, no. 1, 2010. Date revised - 2013-05-01.

[40] L. P. McGuire and M. B. Fenton, "Hitting the wall: Light affects the obstacle avoidance ability of free-flying little brown bats (myotis lucifugus)," *Acta Chiropterologica*, vol. 12, no. 1, pp. 247–250, 2010.

[41] J. W. Bradbury and F. Nottebohm, "The use of vision by the little brown bat, myotis lucifugus, under controlled conditions," *Animal Behaviour*, vol. 17, Part 3, no. 0, pp. 480–485, 1969.

[42] J. Chase and R. A. Suthers, "Visual obstacle avoidance by echolocating bats," *Animal Behaviour*, vol. 17, Part 2, no. 0, pp. 201–207, 1969.

[43] M. V. Srinivasan, J. S. Chahl, K. Weber, S. Venkatesh, M. G. Nagle, and S. W. Zhang, "Robot navigation inspired by principles of insect vision," *Robotics and Autonomous Systems*, vol. 26, no. 2–3, pp. 203–216, 1999.

[44] B. Falk, L. Jakobsen, A. Surlykke, and C. F. Moss, "Bats coordinate sonar and flight behavior as they forage in open and cluttered environments," *The Journal of Experimental Biology*, vol. 217, no. 24, pp. 4356–4364, 2014.

[45] A. Surlykke, K. Ghose, and C. F. Moss, "Acoustic scanning of natural scenes by echolocation in the big brown bat, eptesicus fuscus," *Journal of Experimental Biology*, vol. 212, no. 7, pp. 1011–1020, 2009.

[46] Y. Gustafson and H. U. Schnitzler, "Echolocation and obstacle avoidance in the hipposiderid batasellia tridens," *Journal of comparative physiology*, vol. 131, no. 2, pp. 161–167, 1979.

[47] R. A. Grummon and A. Novick, "Obstacle avoidance in the bat, macrotus mexicanus," *Physiological Zoology*, vol. 36, no. 4, pp. 361–369, 1963.

[48] R. Galambos and D. R. Griffin, "Obstacle avoidance by flying bats: The cries of bats," *Journal of Experimental Zoology*, vol. 89, no. 3, pp. 475–490, 1942.

[49] H. R. Goerlitz, D. Genzel, and L. Wiegrebe, "Bats' avoidance of real and virtual objects: Implications for the sonar coding of object size," *Behavioural Processes*, vol. 89, no. 1, pp. 61–67, 2012.

[50] D. R. Griffin and D. Thompson, "Echolocation by cave swiftlets," *Behavioral Ecology and Sociobiology*, vol. 10, no. 2, pp. 119–123, 1982.

[51] D. R. Griffin, "Acoustic orientation in the oil bird, steatornis," *Proceedings of the National Academy of Sciences of the United States of America*, vol. 39, no. 8, pp. 884–893, 1953.

[52] K. Ghose, T. K. Horiuchi, P. S. Krishnaprasad, and C. F. Moss, "Echolocating bats use a nearly time-optimal strategy to intercept prey.," *Plos Biology*, vol. 4, no. 5, p. e108, 2006.

[53] M. L. Avery, P. F. Springer, and N. S. Dailey, *Avian Mortality at Man-Made Structure: An Annotated Bibliography (Revised).* US Fish and Wildlife Services, 1980.

[54] H. B. Wood, "Fractures among birds," *Bird-Banding*, vol. 12, pp. 68–72, Apr 1941.

[55] G. E. Concepts and N. D. of Environmental Conservation, "Birds and bats: Potential impacts and survey techniques," *NYS Energy Research and Development Authority*, Oct 2005.

[56] J. J. Gibson, "Perception of the visual world.," *Science*, vol. 113, May 1951.

[57] V. Sezer and M. Gokasan, "A novel obstacle avoidance algorithm: "follow the gap method".," *Robotics and Autonomous Systems*, vol. 60, pp. 1123 – 1134, 2012.

[58] O. Khatib, "Real-time obstacle avoidance for manipulators and mobile robots.," in *IEEE International Conference on Robotics and Automation (ICRA)*, (St. Louis, MO), pp. 500–05, 1985.

[59] C. I. Connolly, J. B. Burns, and R. Weiss, "Path planning using laplace's equation," in *Robotics and Automation, 1990. Proceedings., 1990 IEEE International Conference on*, pp. 2102–2106 vol.3, May 1990.

[60] P. Vadakkepat, T.-H. Lee, and L. Xin, *Autonomous Robotic Systems: Soft Computing and Hard Computing Methodologies and Applications*, ch. Evolutionary Artificial Potential Field — Applications to Mobile Robot Path Planning, pp. 217–232. Heidelberg: Physica-Verlag HD, 2003.

[61] N. Michael, S. Shen, K. Mohta, Y. Mulgaonkar, V. Kumar, K. Nagatani, Y. Okada, S. Kiribayashi, K. Otake, K. Yoshida, K. Ohno, E. Takeuchi, and S. Tadokoro, "Collaborative mapping of an earthquake-damaged building via ground and aerial robots.," *Journal of Field Robotics*, vol. 29, no. 5, pp. 832 – 841, 2012.

[62] B. Siciliano and O. Khatib, *Springer Handbook of Robotics*. Secaucus, NJ, USA: Springer-Verlag New York, Inc., 2007.

[63] É. Marchand and F. Chaumette, "Feature tracking for visual servoing purposes.," *Robotics and Autonomous Systems*, vol. 52, no. 1, pp. 53–70, 2005.

[64] R. Mebarki, V. Lippiello, and B. Siciliano, "Nonlinear visual control of unmanned aerial vehicles in gps-denied environments," *IEEE Transactions on Robotics*, vol. 31, pp. 1004–1017, Aug 2015.

[65] S. Kim, H. Seo, S. Choi, and H. J. Kim, "Vision-guided aerial manipulation using a multirotor with a robotic arm," *IEEE/ASME Transactions on Mechatronics*, vol. 21, pp. 1912–1923, Aug 2016.

[66] D. Lee, H. Lim, and H. J. Kim, "Obstacle avoidance using image-based visual servoing integrated with nonlinear model predictive control," in *2011 50th IEEE Conference on Decision and Control and European Control Conference*, pp. 5689–5694, Dec 2011.

[67] T. A. Sarmiento and R. R. Murphy, "Artificial potential field implementation of flying animal gap-aiming behavior in 3d," in *IEEE International Symposium on Safety, Security, and Rescue Robotics*, 2016.

[68] https://3dr.com/solo-drone/specs/, 2016.

[69] https://pixhawk.org, 2016.

[70] R. C. Arkin and R. R. Murphy, "Autonomous navigation in a manufacturing environment," *IEEE Transactions on Robotics and Automation*, vol. 6, pp. 445–454, Aug 1990.

[71] J. Rosenblatt, "Damn: A distributed architecture for mobile navigation.," *Journal of Experimental and Theoretical Artificial Intelligence*, vol. 9, no. 2-3, pp. 339–360, 1997.

[72] N. D. Muñoz, J. A. Valencia, and N. Londoño, "Evaluation of navigation of an autonomous mobile robot," in *Proceedings of the 2007 Workshop on Performance Met-*

rics for Intelligent Systems, PerMIS '07, (New York, NY, USA), pp. 15–21, ACM, 2007.

[73] W. Nowak, A. Zakharov, S. Blumenthal, and E. Prassler, "Benchmarks for mobile manipulation and robust obstacle avoidance and navigation," *BRICS Deliverable, D31*, 2010.

[74] B. Mettler, Z. Kong, C. Goerzen, and M. Whalley, "Benchmarking of obstacle field navigation algorithms for unmanned helicopters.," in *Annual Forum Proceedings - American Helicopter Society*, vol. CONF 66, pp. 1936 – 1953, 2010.

[75] https://3dr.com/blog/solo-specs-just-the-facts-14480cb55722/.

[76] A. C. Woods, H. M. Lay, and Q. P. Ha, "A novel extended potential field controller for use on aerial robots," in *IEEE International Conference on Automation Science and Engineering (CASE)*, pp. 286–291, Aug 2016.

[77] A. H. J. de Ruiter and S. Owlia, "Autonomous obstacle avoidance for fixed-wing unmanned aerial vehicles," *The Aeronautical Journal*, vol. 119, no. 1221, pp. 1415–1436, 2015.

[78] Y. Koren and J. Borenstein, "Potential field methods and their inherent limitations for mobile robot navigation," in *IEEE International Conference on Robotics and Automation*, pp. 1398–1404 vol.2, Apr 1991.